



Cite as  
Nano-Micro Lett.  
(2024) 16:37

## Advances of Electrochemical and Electrochemiluminescent Sensors Based on Covalent Organic Frameworks

Yue Cao<sup>1,2</sup>, Ru Wu<sup>2</sup>, Yan-Yan Gao<sup>1</sup>, Yang Zhou<sup>1</sup> ✉, Jun-Jie Zhu<sup>2</sup> ✉

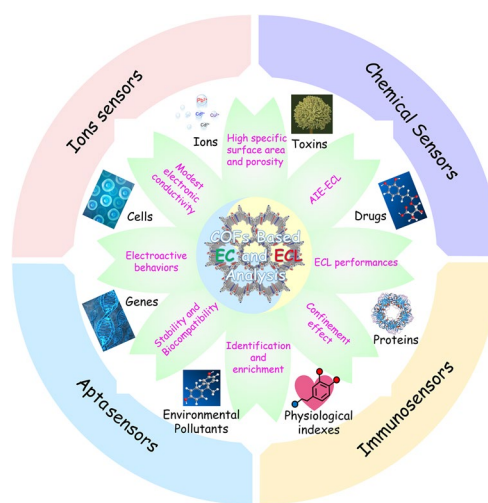
Received: 30 June 2023  
Accepted: 19 October 2023  
Published online: 30 November 2023  
© The Author(s) 2023

### HIGHLIGHTS

- Covalent organic frameworks (COFs) show enormous potential for building high-performance electrochemical sensors due to their high porosity, large specific surface areas, stable rigid topology, ordered structures, and tunable pore microenvironments.
- The basic properties, monomers, and general synthesis methods of COFs in the electroanalytical chemistry field are introduced, with special emphasis on their usages in the fabrication of chemical sensors, ions sensors, immunosensors, and aptasensors.
- The emerged COFs in the electrochemiluminescence realm are thoroughly covered along with their preliminary applications.

**ABSTRACT** Covalent organic frameworks (COFs), a rapidly developing category of crystalline conjugated organic polymers, possess highly ordered structures, large specific surface areas, stable chemical properties, and tunable pore microenvironments. Since the first report of boroxine/boronate ester-linked COFs in 2005, COFs have rapidly gained popularity, showing important application prospects in various fields, such as sensing, catalysis, separation, and energy storage. Among them, COFs-based electrochemical (EC) sensors with upgraded analytical performance are arousing extensive interest. In this review, therefore, we summarize the basic properties and the general synthesis methods of COFs used in the field of electroanalytical chemistry, with special emphasis on their usages in the fabrication of chemical sensors, ions sensors, immunosensors, and aptasensors. Notably, the emerged COFs in the electrochemiluminescence (ECL) realm are thoroughly covered along with their preliminary applications. Additionally, final conclusions on state-of-the-art COFs are provided in terms of EC and ECL sensors, as well as challenges and prospects for extending and improving the research and applications of COFs in electroanalytical chemistry.

**KEYWORDS** Covalent organic frameworks; Electrochemistry; Electrochemiluminescence; Sensors



Yue Cao and Ru Wu have contributed equally to this work.

✉ Yang Zhou, [iamyangzhou@njupt.edu.cn](mailto:iamyangzhou@njupt.edu.cn); Jun-Jie Zhu, [jjzhu@nju.edu.cn](mailto:jjzhu@nju.edu.cn)

<sup>1</sup> Key Laboratory for Organic Electronics and Information Displays (KLOEID) and Institute of Advanced Materials (IAM), Nanjing University of Posts and Telecommunications (NJPT), Nanjing 210023, People's Republic of China

<sup>2</sup> State Key Laboratory of Analytical Chemistry for Life Science, School of Chemistry and Chemical Engineering, Nanjing University, Nanjing 210023, People's Republic of China



## 1 Introduction

Since the discovery of boron-containing covalent organic frameworks (COFs) by Yaghi's group in 2005 [1], this new class of porous crystalline materials has attracted widespread attention across several scientific communities [2–5]. Typically, COFs are formed via the polymerization of light elements, which are known to form robust covalent bonds in well-established and useful topologies [2, 3]. As a kind of porous polymer, crystalline COFs are characterized by a large specific surface area, high porosity, stable rigid topology, and tunable pore structure [4, 5]. Thus, with the rapid development of synthetic strategies and the properties disclosure of COFs in all aspects, a huge surge has emerged in their research and usage, especially in the fields of sensing, catalytic technology, optoelectronic devices, energy storage, pollutants treatment, etc. [6–11].

Electrochemistry has been recognized as a versatile analytical tool over the past few decades and remains competitive in the face of growing demands in life analysis, environmental monitoring, and food inspection [12, 13]. Known for superiorities in high sensitivity, low cost, fast response, simple equipment, and easy miniaturization, electrochemical (EC) sensors are devices that convert EC data between target analytes or sensing elements into analytical signals with application values [14–16]. Electrochemiluminescence (ECL), an important branch of EC technology, describes the light-emitting phenomenon initiated by the reactions of electro-generated radicals [17, 18]. During this process, the EC signals are converted into optical outputs, effectively avoiding EC background interference [19]. Since the luminescence source comes from the redox reactions on the electrode surface, ECL requires no external light source, displaying almost zero background [20]. Thus, ECL methodology, with characteristics of high sensitivity, outstanding controllability, and low-cost instruments, has aroused extensive

research interest in clinical diagnosis, environmental monitoring, food analysis, etc. [17–20]. No matter the EC or ECL analysis, however, the essence is an EC reaction, that is, the electron-gain and loss reaction of electroactive species in the vicinity of the electrode [21]. Therefore, the established electrode surfaces afford the analytical performance of EC sensors, which is crucial for improving the key technical indicators such as sensitivity, stability, repeatability, and selectivity [17, 22].

It is known that EC sensors rely most on multifarious electroactive or catalytic materials on the electrodes, even though the EC detection methods are much the same [22–25]. Thus, developing and searching for high-quality electrode materials is particularly significant [26–28]. Microporous frameworks, such as inorganic zeolites, metal–organic frameworks (MOFs) [29–34], and organic COFs with high porosity and crystallinity are demonstrated to significantly enhance the analytical performance of EC sensors [35, 36]. Each one has its own superiorities and unique selling points [37–42], and their comparisons are summarized in Table 1 [43–45]. Thereinto, COFs as a brand-new category of porous crystalline materials have rapidly become a study focus in this area. The essence is that the super-micropores, high specific surface area, excellent stability, and modest conductivity of COFs guarantee sufficient active sites and favorable energy/mass transfer, while remarkable diversity and designability of the pore size, skeleton structure, and composition can regulate their EC behaviors.

Considering the great potential of the emerging COFs for building high-performance EC devices [45], this review primarily focuses on the corresponding analysis usages in electroanalytical chemistry (Fig. 1). To the best of our knowledge, there are only a few reviews partly regarding COFs in EC sensing [46–49], and no specific review that describes the role of COFs in the ECL domain to date. Hence, this review aims to make a comprehensive summary

**Table 1** Comparisons of the microporous frameworks of zeolites, MOFs, and COFs

Materials	Micropore	Crystallinity	Stability	Conductivity	Diversity and designability	Solubility	Unique selling points	Research status
Zeolites	Ultra-micropores	Very high	Good	Poor	Good	No	Low cost; stability; commercialization	Active
MOFs	Ultra-micropores	Very high	Poor to good	Poor	Excellent	No	Precise control; ions centers	Hot
COFs	Super-micropores	Modest to high	Excellent	Modest	Excellent	No	Easy regulation; stability; organic	Very hot

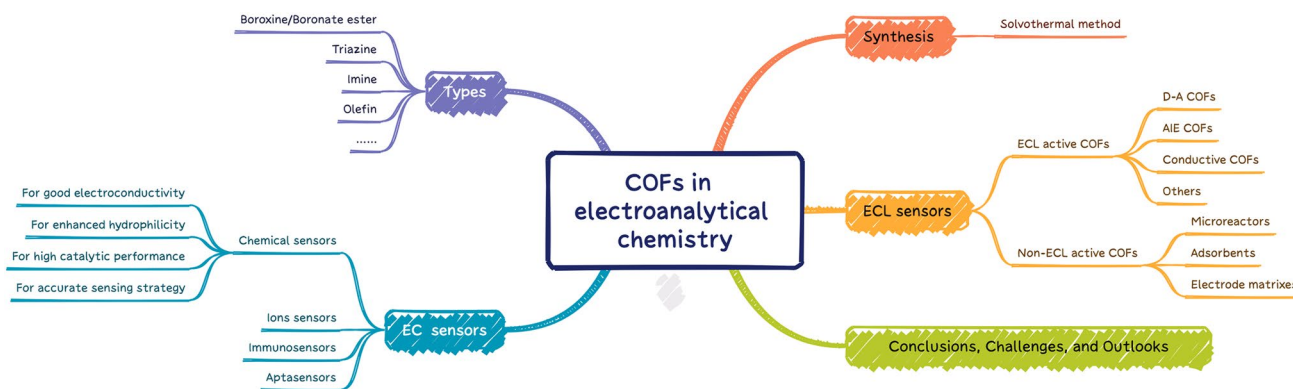


**Fig. 1** Flow chart representing the contents review article

of the reports on COFs in electroanalytical chemistry in the last few years. We summarize the basic characteristics, monomers, and synthesis methods of COFs used in this field. Then, we introduce the EC analytical applications based on functional COFs systematically, including the fabrication of chemical sensors, ions sensors, immunosensors, and aptasensors. Also, COFs directly designed as ECL active emitters and non-ECL active matrixes, as well as their preliminary ECL sensing applications, are further highlighted. Finally, we discuss the challenges and future trends that COFs will face in the field of electroanalytical chemistry.

## 2 Basic Characteristics and Synthetic Methods

Thanks to several impressive reviews on the structural features and synthesis of COFs [2, 3, 5], deep dives into this part will be attempted only regarding COFs in terms of electroanalytical chemistry in this review. Generally, COFs are created by the polymerization of monomers with symmetric reactive groups following specific geometries. During condensation, covalent bonds are spatially confined in either a two- or three-dimensional (2D or 3D) manner or geometrically directed to generate extended and ordered 2D or 3D crystal structures [50, 51]. Metal ions coordination or functional groups can be predesigned into the motifs or introduced through post-modification [6]. Moreover, the presence of heteroatoms within COFs creates special microenvironments for redox-active centers or specific target binding [52, 53]. As such, COFs will advance fundamental understanding and applications to shine in the field of EC analysis.

Nowadays, various types of COFs are reported based on their dynamic covalent bonds, such as boronate ester, imine, olefin,  $\beta$ -ketoenamine, hydrazine, azine, and enamine [2–5, 54]. To the best of our knowledge, the formula of the monomers and their abbreviations used for the construction of COFs-based EC sensors are collected in Fig. 2B, mainly containing aldehyde, amino, cyano, triazine, hydroxyl, carbonyl, and boronic acid groups. The earliest reported boroxine/boronate ester-based COFs might be not stable enough to obtain available EC sensors in aqueous solutions or humid environments because of the electron-deficient nature of boron [1]. Triazine-containing COFs, also referred as covalent triazine skeletons, can be created by cyclic trimerization/hydroxyl aldol condensation reactions of nitrile. In comparison with boron-COFs, they have better stability and several EC usages, but they are commonly synthesized under harsh reaction conditions and with poor crystallinity [55, 56]. The imine-linked COFs are Schiff bases formed by condensation of amino and aldehyde groups, which have excellent crystallinity and structural regularity [57]. In particular, COFs with the imine linkage exhibit good chemical and thermal stability [4, 23]. For example, Xu et al. designed a porous imine-based COF with remarkable stability against water, strong bases, and strong acids by incorporating methoxy motifs into pore skeletons to enhance the interlayer interactions [4]. Until now, imine is still the most reported linkage in COFs preparation for EC sensing applications. Nevertheless, the electrical conductivity of these all-organic COFs is still limited due to the poor charge transfer ability of the linkages between the aromatic motifs [58]. The  $sp^2$  carbon-conjugated COFs with olefin linkages allow for acceptable electrical conductivity, beneficial to constructing

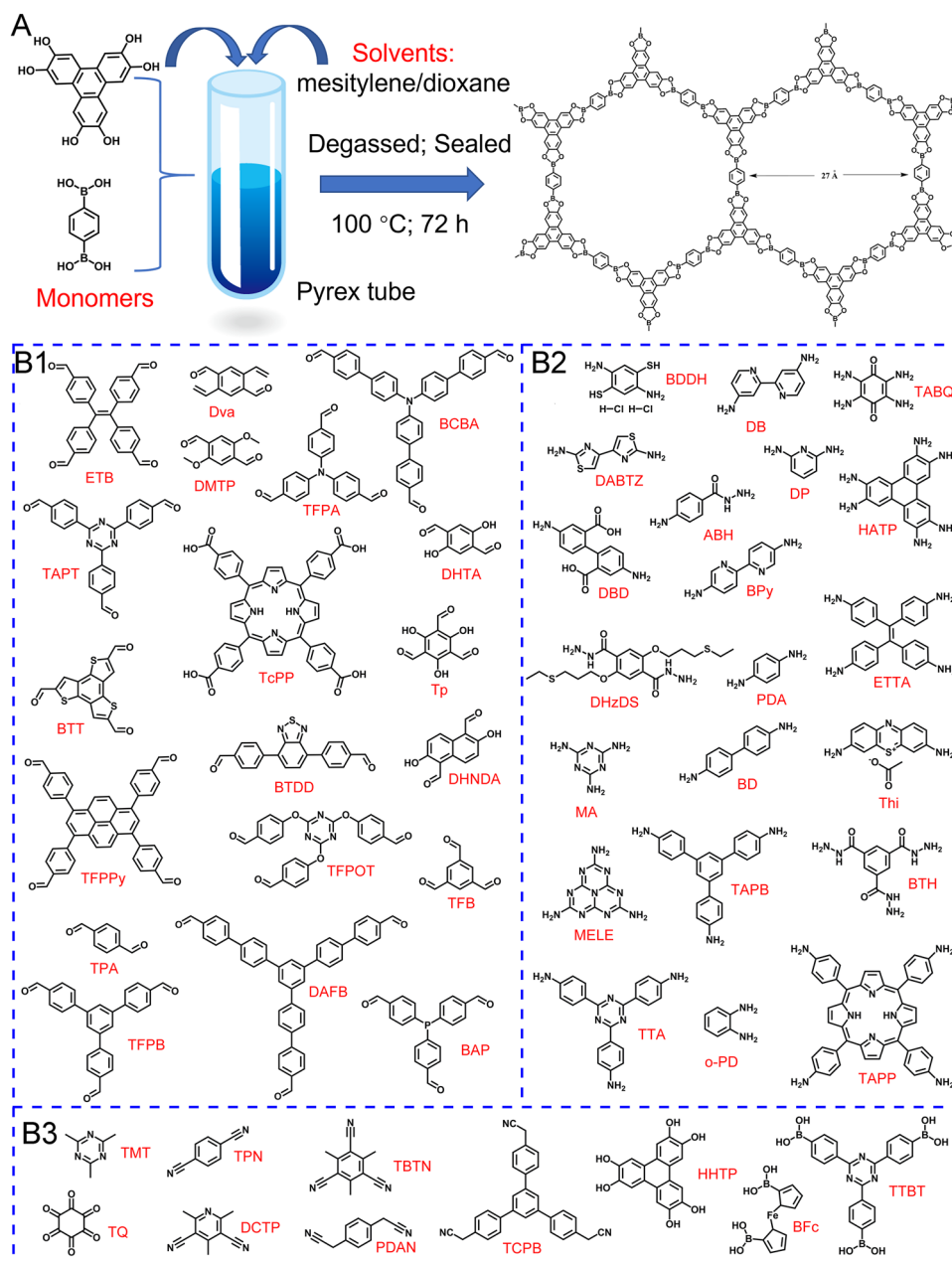


**Fig. 2** **A** The synthesis diagram of the boronate ester-linked COFs via a traditional solvothermal method; Summary of the **B1** aldehyde, **B2** amino, and **B3** other monomers for the synthesis of COFs reported in electroanalytical chemistry

EC sensors [59]. For the reader's convenience, Table 2 summarizes the monomers and linkages of idiographic COFs in EC sensors.

At present, most COFs applied in the EC sensing scope are still dominated by a traditional solvothermal synthetic method [105]. Figure 2A depicts the synthesis diagram of the first reported COF products with the triboronate ester linkage

as an example [1]. Briefly, the reactant monomers, catalysts, and solvents are uniformly mixed in a Pyrex tube, possibly with the aid of sonication. Subsequently, this charged tube is flash-frozen with liquid nitrogen and degassed by a pump. Undergoing multiple freeze–pump–thaw cycles to remove oxygen, it was sealed under a vacuum. The crude products are produced at a suitable temperature for some time, and

**Table 2** Summary of main basic characteristics of various COFs and their EC sensing applications

	COFs	Linkages	Monomers	Derived composites	EC methods	Analytes	Limit of detection	Refs.
Chemical sensors	COF <sub>TAPB-TPA</sub>	Imine	TAPB, TPA	COF/NH <sub>2</sub> -CNTs	DPV	Furazolidone	77.5 nM	[60]
	COF <sub>BTH-Tp</sub>	$\beta$ -ketoenamine	BTH, Tp	COF/NH <sub>2</sub> -CNTs	DPV	Nitrofural	3.2 nM	[61]
	COF <sub>TAPB-Dva</sub>	Imine	TAPB, Dva	COF@graphitized MWCNTs	DPV	Diuron	0.08 $\mu$ M	[62]
	COF <sub>BD-TFPPy</sub>	Imine	BD, TFPPy	COF/MWCNTs	DPV	Catechol, hydroquinone	0.36, 0.38 $\mu$ M	[63]
	COF <sub>TAPB-TFPB</sub>	Imine	TAPB, TFPB	COF/Ox-MWCNTs	DPV	Dopamine, uric acid	0.073, 0.063 $\mu$ M	[64]
	COF <sub>ABH-TFPOT</sub>	Imine	ABH, TFPOT	COF/polyaniline	DPV	Sulfamethoxazole	0.107 $\mu$ M	[65]
	COF <sub>TAPB-TPA</sub>	Imine	TAPB, TPA	COF/AuNPs	SWV	Enrofloxacin	0.041 $\mu$ M	[66]
	COF <sub>TAPB-DMTP</sub>	Imine	TAPB, DMTP	COF/AuNPs	DPV	Chlorogenic acid	9.5 nM	[67]
	COF <sub>DP-TFPPy</sub>	Imine	DP, TFPPy	COF/AuNPs	DPV	Theophylline, caffeine	0.19, 0.076 $\mu$ M	[68]
	COF <sub>BD-Tp</sub>	Imine	BD, Tp	COF/AuNPs	DPV	Bisphenol A	1 $\mu$ M	[69]
	COF <sub>BD-Tp</sub>	Imine	BD, Tp	COF/PtNPs/MWCNTs	DPV	Tanshinol	0.018 $\mu$ M	[22]
	COF <sub>TAPB-DMTP</sub>	Imine	TAPB, DMTP	COF/AuNPs/MWCNTs	DPV	Doxorubicin	16 nM	[70]
	COF <sub>DHzDS-TFPB</sub>	Imine	DHzDS, TFPB	COF/PtNPs@rGO	DPV	Furazolidone	0.23 $\mu$ M	[71]
	COF <sub>PDA-TFPPy</sub>	Imine	PDA, TFPPy	COF/MWCNT-NH <sub>2</sub> /AuNPs	DPV	Dopamine, uric acid	0.21, 0.29 $\mu$ M	[72]
	COF <sub>TABQ-TQ</sub>	Pyrazine	TABQ, TQ	/	DPV	Guanine, adenine	0.20, 0.33 $\mu$ M	[73]
	COF <sub>DABTZ-Tp</sub>	Imine	DABTZ, Tp	COF/AChE	DPV	Methyl parathion, paraoxon, malathion	0.204, 0.794, 5.37 $\text{pg mL}^{-1}$	[74]
	COF <sub>TTA-Tp</sub>	Imine	TTA, Tp	Post-carboxylation; COF/AuNPs	DPV	Gallic acid, uric acid	0.19, 0.25 $\mu$ M	[75]
	COF <sub>PDA-Tp</sub>	Imine	PDA, Tp	2HP6@AuNPs@CP6@COF	DPV	Sodium picrate	1.7 nM	[76]
	COF <sub>CTF-1</sub>	Triazine	TPN	COF/SOD	i-t	Superoxide radicals	0.5 nM	[55]
	COF <sub>BTH-DHNDA</sub>	Imine	BTH, DHNDA	COF/AChE	CV	Carbaryl	0.16 $\mu$ M	[77]
	COF <sub>ETTA-TPA</sub>	Imine	ETTA, TPA	COF/MPO-11, GOD	DPV	Glucose	4.97 $\mu$ M	[78]
	COF <sub>DBD-TFPB</sub>	Imine	DBD, TFPB	COF/GOD, HRP, AChE	DPV	Glucose, H <sub>2</sub> O <sub>2</sub> , malathion	0.85 $\mu$ M, 2.81 nM, 0.3 $\text{pg L}^{-1}$	[14]
	COF <sub>TAPB-DMTP</sub>	Imine	TAPB, DMTP	Co <sub>3</sub> O <sub>4</sub> @COF	DPV	Tert-butylhydroquinone	0.02 $\mu$ M	[23]
	COF <sub>TAPB-DMTP</sub>	Imine	TAPB, DMTP	FeNi@COF	DPV	Gallic acid	1.3 nM	[79]
	COF <sub>TAPB-DMTP</sub>	Imine	TAPB, DMTP	CuO nanorods@COF	DPV	Dopamine	0.023 $\mu$ M	[80]
	COF <sub>TAPP-TFB</sub>	Imine	TAPP, TFB	COF/Fe <sup>2+</sup>	DPV	H <sub>2</sub> O <sub>2</sub>	2.06 nM	[81]



**Table 2** (continued)

	COFs	Linkages	Monomers	Derived composites	EC methods	Analytes	Limit of detection	Refs.
Ions Sensors	COF <sub>TAPB-DMTP</sub>	Imine	TAPB, DMTP	COF/ $\beta$ -CD polymers/Pd <sup>2+</sup>	DPV	Norfloxacin	0.031 $\mu$ M	[82]
	COF <sub>Thi-TFPB</sub>	Imine	Thi, TFPB	COF/NH <sub>2</sub> -CNTs	DPV	Ascorbic acid	17.68 $\mu$ M	[83]
	COF <sub>Thi-TFPB</sub>	Imine	Thi, TFPB	COF/3D-MC	DPV	Riboflavin	44 nM	[84]
	COF <sub>TTA-DHTA</sub>	Imine	TTA, DHTA	COF/GOD	DPV	H <sub>2</sub> O <sub>2</sub> , glucose	1.70, 0.18 $\mu$ M	[85]
	COF <sub>ETTA-TPA</sub>	Imine	ETTA, TPA	COF/Fc	DPV	H <sub>2</sub> O <sub>2</sub>	0.33 $\mu$ M	[13]
	COF-LZU1	Imine	PDA, TFB	AgNPs/COF	DPV	Bisphenol A, bisphenol S	0.15, 0.15 $\mu$ M	[86]
	COF <sub>TAPB-DMTP</sub>	Imine	TAPB, DMTP	/	DPASV	Pb <sup>2+</sup>	1.9 nM	[52]
	COF <sub>MA-TPA</sub>	Imine	MA, TPA	Fe <sub>3</sub> O <sub>4</sub> NPs@COF/bismuth film	SWASV	Pb <sup>2+</sup>	0.95 nM	[87]
	COF <sub>TAPB-Dva</sub>	Imine	TAPB, Dva	TTC post-modification; graphene	SWASV	Cd <sup>2+</sup> , Pb <sup>2+</sup> , Cu <sup>2+</sup> , Hg <sup>2+</sup>	0.3, 0.2, 0.2, 1.1 $\mu$ g L <sup>-1</sup>	[53]
	COF <sub>TTA-BTT</sub>	Imine	TTA, BTT	/	DPSV	Hg <sup>2+</sup>	0.18 nM	[88]
	COF <sub>MELE-BTDD</sub>	Imine	MELE, BTDD	/	SWASV	Cd <sup>2+</sup> , Pb <sup>2+</sup> , Cu <sup>2+</sup> , Hg <sup>2+</sup>	4.74, 1.23, 1.14, 1.07 nM	[89]
	COF <sub>MA-Tp</sub>	Imine	MA, Tp	/	SWASV	Cd <sup>2+</sup> , Cu <sup>2+</sup> , Pb <sup>2+</sup> , Hg <sup>2+</sup> , Zn <sup>2+</sup>	0.92, 0.45, 0.31, 0.21, 0.53 nM	[90]
	COF <sub>BTLP-1</sub>	Imine	BDDH, TFB	COF/3D-MC	DPSV	Cd <sup>2+</sup> , Pb <sup>2+</sup> , Cu <sup>2+</sup> , Hg <sup>2+</sup>	12.3, 11.8, 18.6, 21.4 nM	[24]
	COF <sub>TAPB-DMTP</sub>	Imine	TAPB, DMTP	COF/TiO <sub>2</sub> -NH <sub>2</sub>	SWCSV	Mn <sup>2+</sup>	0.0283 nM	[91]
	COF <sub>TAPB-DMTP</sub>	Imine	TAPB, DMTP	COF/AuNPs/Ab/HRP	DPV	Cardiac troponin I	1.7 pg mL <sup>-1</sup>	[92]
Immunosensors	COF-LZU1	Imine	PDA, TFB	COF/AuNPs/Ab/TB	SWV	Cardiac troponin I	0.17 pg mL <sup>-1</sup>	[93]
	COF <sub>BD-Tp</sub>	Imine	BD, Tp	Fe <sub>3</sub> O <sub>4</sub> @COF/AuNPs/MB/Ab	DPV	Prostate specific antigen	30 fg mL <sup>-1</sup>	[94]
	COF-LZU1	Imine	PDA, TFB	COF/PtNPs/Ab	DPV	C-reactive protein	0.2 ng mL <sup>-1</sup>	[95]
	COF <sub>TAPB-TPA</sub>	Imine	TAPB, TPA	COF/AuNPs/Ab	DPV	Kidney injury molecule-1	2.0 fg mL <sup>-1</sup>	[96]
	COF <sub>TAPB-DMTP</sub>	Imine	TAPB, DMTP	COF/CuS NPs	DPV	Amyloid- $\beta$ oligomer	0.4 pM	[97]
	COF <sub>TAPB-TPA</sub>	Imine	TAPB, TPA	aptamer/AuNPs@ZnFe <sub>2</sub> O <sub>4</sub> @COF	DPV	Norovirus	0.003 copies mL <sup>-1</sup>	[98]
	COF <sub>Bpy-Tp</sub>	Imine	Bpy, Tp	AuNPs@Ce-COF/aptamer	i-t	Zearalenone	0.389 pg mL <sup>-1</sup>	[99]
	COF <sub>HHTP-BFc</sub>	Imine	HHTP, BFc	COF/aptamer	DPV	Cardiac troponin I	2.6 fg mL <sup>-1</sup>	[100]
	COF <sub>TAPB-DMTP</sub>	Imine	TAPB, DMTP	COF/AuNPs/ aptamer	EIS	Ciprofloxacin	2.34 fg mL <sup>-1</sup>	[101]
	COF <sub>TAPB-DMTP</sub>	Imine	TAPB, DMTP	COF/CNTs/ aptamer	EIS	Atrazine	0.67 pg mL <sup>-1</sup>	[102]
	COF <sub>MA-TFPPy</sub>	Imine	MA, TFPPy	COF/aptamer	EIS	Ampicillin, enrofloxacin	0.04, 6.07 fg mL <sup>-1</sup>	[103]



**Table 2** (continued)

COFs	Linkages	Monomers	Derived composites	EC methods	Analytes	Limit of detection	Refs.
COF <sub>TAPP-TPA</sub>	Imine	TAPP, TPA	COF/aptamer	EIS	EGFR, MCF-7 cells	7.54 fg mL <sup>-1</sup> , 61 cells mL <sup>-1</sup>	[104]
COF <sub>CTF-1</sub>	Triazine	TPN	Co-MOF@COF/ aptamer	EIS	Ampicillin	0.217 fg mL <sup>-1</sup>	[56]

the precipitates are collected, washed, and dried to obtain the final products [47]. Although COFs structure at the macroscopic level can be regulated, this method involves tedious preparation procedures and harsh reaction conditions. Several simplified synthetic methods have been attempted, that are, for example, the preparation using a stainless-steel reactor lined with a Teflon vessel [2, 83, 88, 106], and direct polycondensation under ambient conditions without vacuuming and heating processes [60, 92]. Certainly, exploring facile and green synthetic strategies is a new trend in manufacturing COFs-based EC sensors, such as water-mediated, solid-phase, vapor-assisted, hydrothermal, and micelle-assisted synthesis approaches [107].

### 3 COFs in EC Sensing

Crystalline COFs exhibit prominent advantages in achieving high-performance EC sensing compared with traditional covalent polymers and quite similar MOFs [2–5, 30, 32, 108–111]. First, COF networks built by  $\pi$ -stacking or extended  $\pi$ -conjugated backbones allow fast charge transport along the self-assembled molecular channel and show modest electrical conductivity. Second, the generally high specific surface area endows their high-load capacity of EC-active substances and a large electrode active area. Third, their macrostructures and nanosized pores can be tailored to accommodate specific guests via the non-covalent interaction (i.e., hydrogen bonds,  $\pi$ - $\pi$ , hydrophobic, and electrostatic interactions), facilitating selective identification and enrichment of target molecules. Fourth, electroactive COFs with given redox patterns are utilized to develop accurate ratiometric EC sensing. Fifth, COFs with good flexibility are well distributed on the electrode surface without the assistance of membrane forming-reagents (e.g., Nafion and chitosan). Last but not least, COFs typically exhibit low toxicity, good biocompatibility, as well as high chemical and

thermal stability, benefiting the development of repeatable and reproducible EC sensors, especially for the usages in biosensing. The relevant advances in COFs-based EC sensors including electrode materials, EC methods, analytes, and the limit of detection (LOD) are summarized in Table 2, and several representative ones are described in detail below.

#### 3.1 Chemical Sensors

Chemical sensors are involved in all aspects of life, including physiological check, drug evaluation, food testing, environmental monitoring, etc. [112]. Most chemical molecules have their own characteristic EC redox activities, making them easy and convenient to be directly recognized according to their electro-redox attributes. Thus, versatile sensors by means of EC technologies, especially differential pulse voltammetry (DPV), square wave voltammetry (SWV), and amperometry (*i-t*), have been widely designed for chemical sensing because of their superiorities of sensitivity, portability, automation, and low price [83, 85]. Importantly, highly adaptable structural and functional design, specific recognition, electroactivity, unique catalytic capabilities, as well as inherent natures including high specific surface areas, ordered channels, and acceptable stability, make COFs promising electrode substrates for chemical detection. Thanks to the ample examples of chemical sensors, in this section, these improvement strategies of COFs-based analysis are further classified into the following four parts according to the improvement strategies.

##### 3.1.1 For Good Electroconductivity

Despite these advantages, current COFs as electrode materials are still limited due to their poor affinity and conductivity. Hybridization with carbon materials might be the simplest and most economical way to achieve conductivity



improvement [113]. Carbon nanotubes (CNTs) contain  $sp^2$  hybridized carbon atoms in a graphite sheet-like manner, owning large delocalized  $\pi$  orbitals and high electrical conductivity [60]. Further, mainly through  $\pi$ - $\pi$  stacking, the conjugated COFs can be non-covalently assembled on the outer surface of CNTs. For instance, following an one-pot synthesis at a mild reaction condition,  $\text{COF}_{\text{TAPB-TPA}}$  was immobilized in situ on an  $\text{NH}_2$ -CNTs matrix with the building monomers of 1,3,5-tris(4-aminophenyl)benzene (TAPB) and terephthalaldehyde (TPA). The resultant  $\text{COF}_{\text{TAPB-TPA}}/\text{NH}_2$ -CNTs presented nice conductivity and a large specific surface area, enabling the fabrication of a furazolidone EC sensor with a low LOD of 77.5 nM and acceptable recoveries ranged from 87.8 to 126.9% [60]. A similar work reported the growth of  $\beta$ -ketoenamine-linked  $\text{COF}_{\text{BTH-Tp}}$  on  $\text{NH}_2$ -CNTs by dehydration condensation between benzene-1,3,5-tricarbohydrazide (BTH) and 1,3,5-triformylphloroglucinol (Tp). Based on the composite, an EC sensor displayed excellent performances for nitro-fural detection with a LOD of 3.2 nM [61]. Li et al. proposed an ultrasonic-mediated method for the self-assembly of  $\text{COF}_{\text{TAPB-Dva}}$  (Dva: 2,5-divinylterephthalaldehyde)@graphitized multi-walled CNTs (MWCNTs) via the  $\pi$ - $\pi$  conjugation effect. This silkworm-cocoon-like nanohybrid was further employed for the reliable detection of diuron in food samples, achieving a LOD of 0.08  $\mu\text{M}$  and satisfactory recoveries from 96.40 to 103.20% [62]. Besides, conductive polymers can serve as conductive carriers for the in-situ loading of COFs. Using *p*-aminobenzoyl hydrazide (ABH)

and 2,4,6-tris-(4-formylphenoxy)-1,3,5-triazine (TFPOT) as the monomers, Pan et al. accomplished a facile one-pot approach for in-situ growth of  $\text{COF}_{\text{ABH-TFPOT}}$  on the polyaniline, which amplified the response signal of sulfamethoxazole (SMX). This COFs-based EC sensor displayed a broad linear range (1–450  $\mu\text{M}$ ) and a low LOD (0.107  $\mu\text{M}$ ) for SMX, and was used for reliable testing of environmental water samples [65].

Nobel metal nanoparticles (NPs), known for excellence in conductivity, biocompatibility, and catalytic activity [66, 67], can be controllably grown and confined within the regular pore channels of COFs in a well-dispersed manner, thus fully exploiting the capabilities of COFs. For example, Lu and co-workers prepared  $\text{COF}_{\text{TAPB-TPA}}/\text{AuNPs}$  via an in-situ growth method for enrofloxacin (ENR) detection. These loaded AuNPs-assisted redox reactions by lowering the overpotential, stabilizing reversibility, and accelerating charge transfer, thereby achieving a low LOD of 0.041  $\mu\text{M}$  and good recoveries of 96.7–102.2% [66]. Similarly, Zhang and her colleagues fabricated an active and repeatable EC sensor for chlorogenic acid measurement based on COFs-supported AuNPs. In this work, AuNPs were prepared by *in-situ* chemical reduction and landed on the  $\text{COF}_{\text{TAPB-DMTP}}$  (DMTP: 2,5-dimethoxyterephthalaldehyde) surface due to the firm electrostatic absorption of the remaining  $-\text{NH}_2$  of COFs (Fig. 3) [67]. In another work, Guan et al. obtained a new COF by a Schiff-base reaction between 2,6-diaminopyridine (DP) and 4,4',4'',4'''-(pyrene-1,3,6,8-tetrayl)tetrabenzaldehyde (TFPPy) through a tube oven heating program. Further

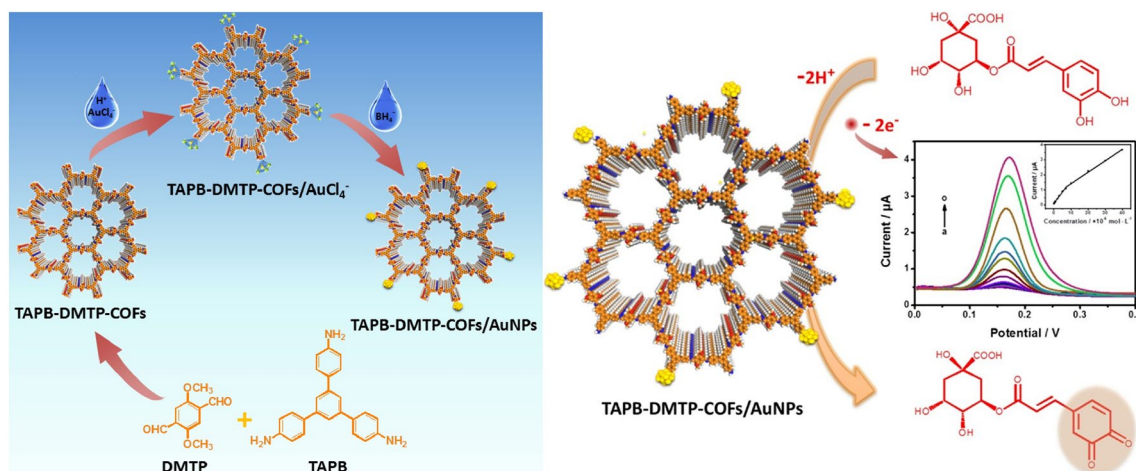


**Fig. 3** Schematic diagrams of the synthesis route for  $\text{COF}_{\text{TAPB-DMTP}}/\text{AuNPs}$  and the resulting EC sensing for chlorogenic acid. Reproduced with permission from Ref. [67]. Copyright (2018) Elsevier



compounded with AuNPs, the resultant  $\text{COF}_{\text{DP-TFPPy}}/\text{AuNPs}$  were directly utilized for the fabrication of a sensitive EC sensor to evaluate theophylline and caffeine in compound paracetamol capsules and black tea samples, and the LODs were 0.19 and 0.076  $\mu\text{M}$ , respectively [68].

The synergy of multiple conductive species usually contributes to better EC activity. For instance, Zhang et al. synthesized the spherical  $\text{COF}_{\text{BD-Tp}}$  (BD: benzidine) by a facile solution-phase method and loaded PtNPs by in-situ chemical reduction of  $\text{H}_2\text{PtCl}_4$ . After further integration of MWCNTs, the resultant ternary composites exhibited outstanding catalytic performance and electrical conductivity, affording effective drug sensing of tanshinol with a sensitivity up to 10.089  $\mu\text{A mM}^{-1}$  and a LOD down to 0.018  $\mu\text{M}$  [22]. Zhao and her colleagues developed an electrode matrix of  $\text{COF}_{\text{TAPB-DMTP}}$  co-decorated with AuNPs and MWCNTs. This dual conductive species-supported COFs sensor exhibited excellent stability, reproducibility, and selectivity for doxorubicin detection with a low LOD of 16 nM [70]. Chen et al. fabricated a paper-based EC sensor for the furazolidone detection based on the nanocomposites of PtNPs/ $\text{COF}_{\text{DHZDS-TFPB}}$  (DHZDS: 2,5-bis (3-(ethyl thiol) propoxy) *p*-benzoyl hydrazine; TFPB: 1,3,5-tris(*p*-formylphenyl) benzene)@reduced graphene oxide (rGO) [71]. In addition, Guan et al. established an EC sensing platform based on the composite of  $\text{COF}_{\text{PDA-TFPPy}}$ , MWCNTs, and AuNPs. In this work,  $\text{COF}_{\text{PDA-TFPPy}}$  was prepared by aminaldehyde condensation between 1,4-phenylenediamine (PDA) and TFPPy. The synergy of two EC active substances endowed this COFs-based biosensor with high conductivity, extraordinary stability, and large specific surface area, thus achieving simultaneous detection of uric acid (UA) and dopamine (DA) with LODs of 0.29 and 0.21  $\mu\text{M}$ , respectively [72].

Additionally, conductive COFs can be built directly for chemical sensors. For example, Pan et al. prepared  $\text{COF}_{\text{TABQ-TQ}}$  via a condensation reaction of tetraaminobenzoquinone (TABQ) and triquinoyl (TQ). This nitrogen-rich COF presented high crystallinity and good electrical conductivity ( $6.06 \times 10^{-3} \text{ S cm}^{-1}$ ), which was directly employed for the simultaneous analysis of guanine and adenine. The LODs were as low as 0.20 and 0.33  $\mu\text{M}$ , respectively [73]. Wei and co-workers developed an interfacial perturbation growth method to obtain an ultrathin ( $\approx 1.95 \text{ nm}$ ) nitrogen and sulfur-rich bithiazole-based 2D-COF nanosheets (NSs) using the monomers of 2,2'-diamino-4,4'-bithiazole (DABTZ) and Tp. Owing to their remarkable electrical

conductivity and abundant edge unsaturated sites, a high-performance biosensor was fabricated with acetylcholinesterase (AChE) as the biometric element for effective monitoring of organophosphorus pesticides [74].

### 3.1.2 For Enhanced Hydrophilicity

Since COFs are mostly composed of hydrophobic units, their poor hydrophilicity hinders efficient dispersion and causes weak contact between substances and reaction centers, inevitably affecting their EC activity and stability. To solve this problem, Lin's group first prepared N, O-rich  $\text{COF}_{\text{TTA-Tp}}$  through a condensation reaction of 4,4',4''-(1,3,5-triazine-2,4,6-triyl) trianiline (TTA) and Tp. Post-carboxylation was adopted for enhanced hydrophilicity, supplying sufficient electron donors of O and N heteroatoms. Then,  $\text{HAuCl}_4$  was attached and reduced in situ to anchor highly dispersed AuNPs. Meanwhile, the decorated  $-\text{COOH}$  showed a greater affinity for gallic acid (GA) than for UA through hydrogen bonding, resulting in their oxidation peaks being separated on the sensor. Accordingly, the constructed sensor realized simultaneous analysis of GA and UA, displaying wide linear responses (1–175  $\mu\text{M}$ ; 1–150  $\mu\text{M}$ ) and low LODs (0.19 and 0.25  $\mu\text{M}$ ), respectively (Fig. 4) [75]. In another work, AuNPs were immobilized on  $\text{COF}_{\text{PDA-Tp}}$  via supramolecular host–guest recognition of pillar [n]arenes. Specifically, macrocyclic hosts of dihydroxylatopillar [6]arene (2HP6) decorated AuNPs (2HP6@AuNPs) were prepared via in-situ reduction. Next, 2HP6@AuNPs were recognized on the cationic pillar [6]arene (CP6)@ $\text{COF}_{\text{PDA-Tp}}$ . The final heterogeneous composites of 2HP6@AuNPs@CP6@ $\text{COF}_{\text{PDA-Tp}}$  with enhanced hydrophilicity were utilized for rapid EC monitoring of sodium picrate by virtue of the electrocatalysis of AuNPs, the recognition and enrichment of 2HP6 and CP6, as well as the outstanding supporting of  $\text{COF}_{\text{PDA-Tp}}$  [76].

### 3.1.3 For High Catalytic Performance

Enzymatic EC biosensors have received special attention because of the high efficiency and specificity of enzymatic reactions [14]. Nevertheless, native enzymes are vulnerable and prone to aggregation and inactivation during the construction and storage of sensors. Thus, immobilizing enzymes on COFs-supported matrices makes it possible to



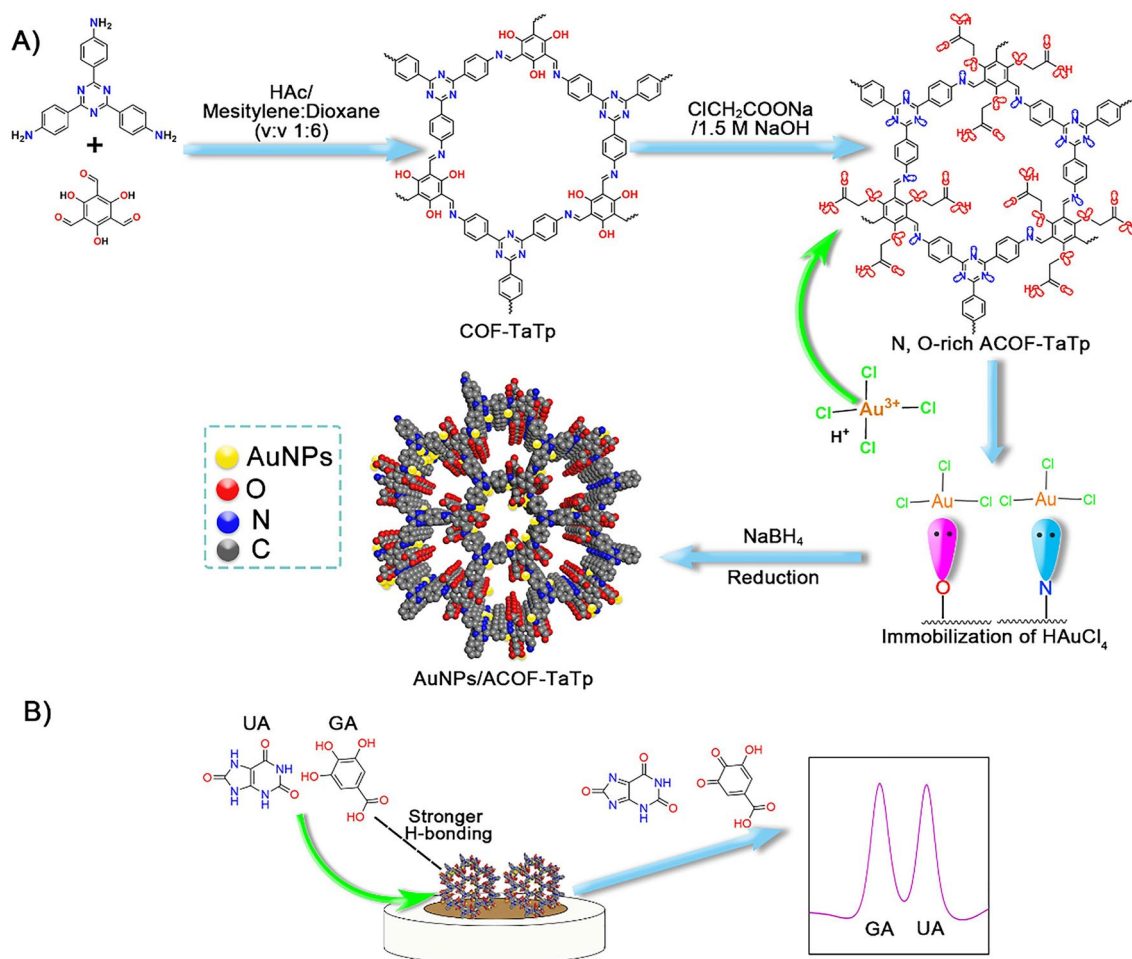


**Fig. 4** Schematic illustrations of the synthesis route for hydrophilic COF<sub>TTA-Tp</sub>/AuNPs and the resulting simultaneous EC sensing of GA and UA. Reproduced with permission from Ref. [75]. Copyright (2021) Elsevier

act synergically for both properties and advantages, sufficiently maintaining bioactivity, and distribution of enzymes. Yildirim et al. synthesized 2D triazine-based COF<sub>CTF-1</sub> through cyclic trimerization using a single terephthalonitrile (TPN) monomer. Based on COF<sub>CTF-1</sub> as the enzymatic support and superoxide dismutase (SOD) as the recognition element, an EC biosensor enabled the inspection of superoxide radicals in clinical samples with a 0.5 nM detection limit [55]. Xiao et al. covalently coupled AChE with the N, O-rich COF<sub>BTH-DHND</sub> (DHND: 2,6-dialdehyde-1,5-dihydroxynaphthalene). Further using anionic [Fe(CN)<sub>6</sub>]<sup>3-/4-</sup> as the sensing indicator, a turn-off EC biosensor based on a flexible carbon paper electrode enabled the carbaryl detection with a low LOD of 0.16 μM [77]. Wang et al. utilized the dual-pore COF<sub>ETTA-TPA</sub> (ETTA: 4,4',4'',4'''-(ethane-1,1,2,2-tetrayl)

tetraaniline) to carry double enzymes of microperoxidase-11 (MPO-11) and glucose oxidase (GOD) for ratiometric EC biosensing of glucose, and the LOD was down to 4.97 μM. In this work, through pore encapsulation and hydrogen bonding, the two enzymes were well supported in different-sized pores of COF<sub>ETTA-TPA</sub>, further allowing their firm attachments onto the electrode surface [78].

Although COFs can indeed protect enzymes from harsh conditions, the micropores of COFs restrict the free conformation of enzymes, which inevitably affects their catalytic activity. To improve the freedom of the enzyme configuration, Liang et al. designed a multienzyme microcapsule with a COF shell and a 600 nm-sized cavity to encapsulate native enzymes. Specifically, three model enzymes of AChE, horseradish peroxidase (HRP), and GOD were first

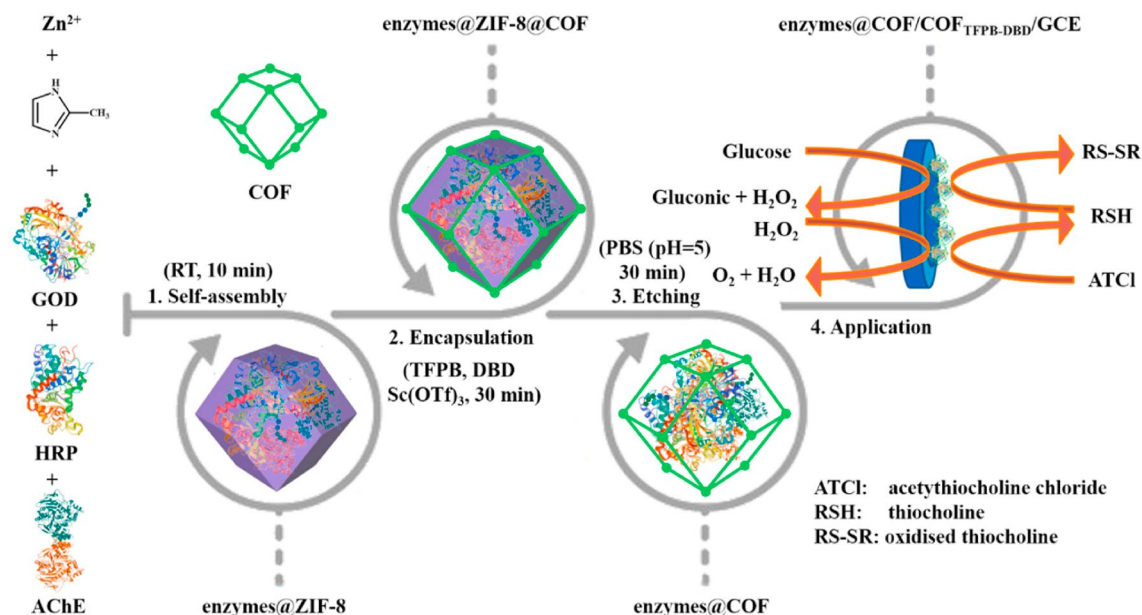


**Fig. 5** Schematic diagrams of the synthesis and usage of a multienzyme microcapsule. Reproduced with permission from Ref. [14]. Copyright (2021) Elsevier

loaded into zeolitic imidazolate framework-8 (ZIF-8). Subsequently, a robust COF<sub>DBD-TFPB</sub> shell was grown in situ outside the enzymes@ZIF-8 with 4,4'-diaminobiphenyl-2,2'-dicarboxylic acid (DBD) and TFPB via amine-aldehyde condensation. Ultimately, ZIF-8 was etched away to form a cavity loaded with multienzymes capable of free conformation. In comparison with those enzymes roughly stacked on the electrode surface, the biosensor constructed with this multienzyme microcapsule displayed superior catalytic performances, and the LODs achieved 0.85  $\mu\text{M}$ , 2.81 nM, and 0.3  $\text{pg L}^{-1}$  for glucose, H<sub>2</sub>O<sub>2</sub>, and malathion detection, respectively (Fig. 5) [14].

Some transition metal oxides and complexes also possess mimic catalytic centers without being limited by the fragility of natural enzymes any more. To avoid aggregation, these centers can be doped into the COFs with good dispersion and unique catalytic activity for non-enzymatic EC sensing. For example, Chen's group proposed a shape-tailored controlled assembly method for growing COF<sub>TAPB-DMTP</sub> on the Co<sub>3</sub>O<sub>4</sub> dodecahedrons. The core-shell composite exhibited uniform size, ultrahigh effective surface area, and excellent thermochemical stability, thus affording the tert-butylhydroquinone (TBHQ) EC sensing with a LOD as low as 0.02  $\mu\text{M}$ . In this architecture, the Co<sub>3</sub>O<sub>4</sub> core guaranteed the superior electronic and catalytic attributes, and 2D COF<sub>TAPB-DMTP</sub>

with multilayered columnar channels facilitated the facile shuttling of TBHQ toward the active Co<sup>3+</sup> sites (Fig. 6A) [23]. In addition, Zha et al. synthesized a core-shell structured FeNi@COF<sub>TAPB-DMTP</sub> nanocomposite with outstanding EC oxidation response toward GA and realized its sensing accordingly [79]. This group also prepared a similar CuO nanorods@COF<sub>TAPB-DMTP</sub> core-shell composite for DA detection with a LOD of 0.023  $\mu\text{M}$  [80].

Iron-porphyrin with Fe<sup>3+</sup>/Fe<sup>2+</sup> electroactive centers exhibits peroxidase biomimetic activity, which can catalyze many EC reactions, such as the reduction of O<sub>2</sub>, H<sub>2</sub>O<sub>2</sub>, and phenolic oxides. For instance, Xie et al. prepared an iron-porphyrin-based COF with monomers of 1,3,5-triformylbenzene (TFB) and 5,10,15,20-tetrakis (4-aminophenyl)-21H,23H-porphine (TAPP) via an aldehyde-ammonia reaction. After the post-chelation with Fe<sup>2+</sup>, the resultant COF<sub>TAPP-TFB</sub>/Fe<sup>2+</sup> served as a mimic peroxidase with remarkable EC redox and proton activity, enabling enzyme-free evaluation of H<sub>2</sub>O<sub>2</sub> and pH (Fig. 6B) [81]. Chu et al. prepared three 2D metalloporphyrin COFs by altering the central metal atoms of Fe, Mn, and Cu. The authors demonstrated that the Fe porphyrin-COF/GCE sensor displayed the best electrocatalytic performance in the EC sensing of butylated hydroxy anisole [114]. In addition to porphyrin, some metal ions can also act as catalysts directly. Zhang

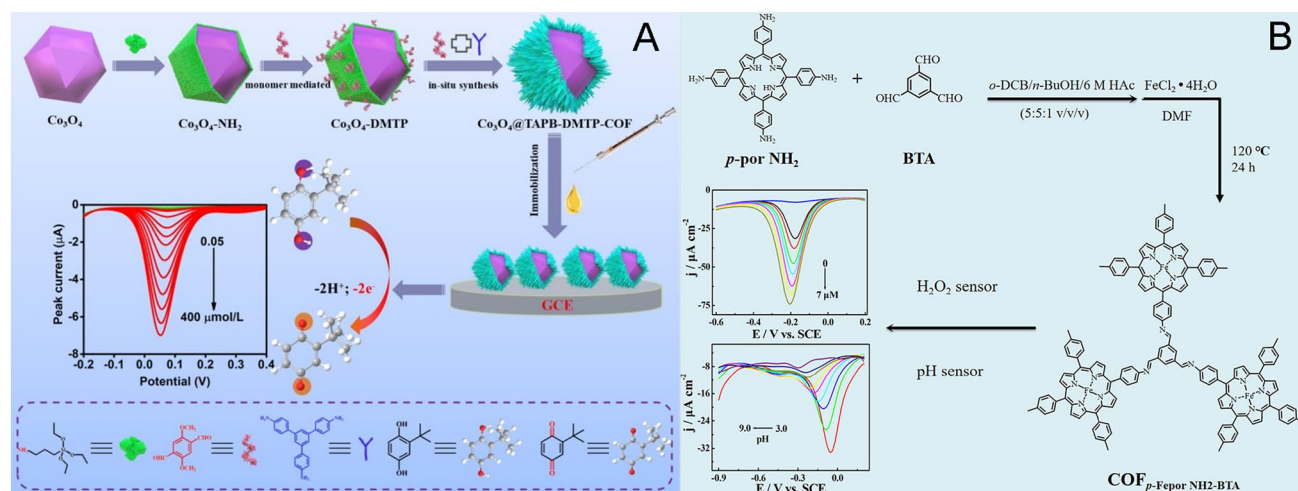


**Fig. 6** Schematic illustrations of the preparation routes and EC sensing applications of **A**  $\text{Co}_3\text{O}_4@\text{COF}_{\text{TAPB-DMTP}}$  and **B**  $\text{COF}_{\text{TAPP-TFB}}/\text{Fe}^{2+}$ . Reproduced with permission from Refs. [23, 81] Copyright (2021, 2020) Elsevier

et al. functionalized  $\text{COF}_{\text{TAPB-DMTP}}$  with  $\beta$ -cyclodextrin ( $\beta$ -CD) porous polymers and the catalytic  $\text{Pd}^{2+}$  element to fabricate a non-enzyme EC sensor for norfloxacin drug checking, showing two linear ranges of 0.08–7.0  $\mu\text{M}$  and 7.0–100.0  $\mu\text{M}$  with a LOD of 0.031  $\mu\text{M}$  [82].

### 3.1.4 For Accurate Sensing Strategy

Ratiometric EC sensors based on two electrical signals are considered a significant advance due to their self-calibration, which can effectively avoid the errors caused by environmental or human factors, ensuring accurate target quantification [115]. It is exciting to note that the multiple redox peaks derived from electroactive COFs can directly serve as the response or reference signals for ratiometric sensing. For example, 2D  $\text{COF}_{\text{Thi-TFPB}}$  was synthesized from thionine (Thi) and TFPB via dehydration condensation and was further enwound by CNTs. With the improved stability and dispersibility, the COFs-supported CNTs exhibited prominent catalytic activity toward the oxidation of ascorbic acid (AA). Meanwhile, a pair of redox peaks assigned to electroactive  $\text{COF}_{\text{Thi-TFPB}}$  were inert to AA. As a result, a ratiometric strategy using the reference EC signal of  $\text{COF}_{\text{Thi-TFPB}}$  allowed for accurate AA sensing with a low LOD of 17.68  $\mu\text{M}$  [83]. This group also grew  $\text{COF}_{\text{Thi-TFPB}}$  vertically on 3D macroporous carbon (3D-MC) to fabricate a carbon paste electrode for dual-signal ratiometric EC assays of riboflavin (RF) with a LOD as low as 44 nM. In this work, target RF molecules

were first oxidized at +0.6 V, and the partially formed oxidized RF ( $\text{RF}_{\text{ox}}$ ) further oxidized  $\text{COF}_{\text{TFPB-Thi}}$  ( $\text{COF}_{\text{ox}}$ ). During the negative potential scanning (+0.6 ~ -0.6 V), the reduction pattern of the composite remained unchanged at -0.23 V, whereas  $\text{COF}_{\text{ox}}$  and  $\text{RF}_{\text{ox}}$  were successively reduced at -0.08 and -0.45 V. Therefore, both the ratio results of  $j_{-0.08}/j_{-0.23}$  V and  $j_{-0.45}/j_{-0.23}$  V can be considered as the response signals, which complemented each other and made the quantification more accurate and reliable (Fig. 7) [84]. In another work,  $\text{COF}_{\text{TTA-DHTA}}$  prepared via aminaldehyde condensation between TTA and 2,5-dihydroxy terethaldehyde (DHTA) was also discovered with multiple redox-active states. Using  $\text{COF}_{\text{TTA-DHTA}}$  as the active material for  $\text{H}_2\text{O}_2$  electrocatalysis, the reduction responses at -0.3 V and -0.5 V were gradually increased with the continuous addition of  $\text{H}_2\text{O}_2$ , while the reduction peak at 0.3 V was nearly kept constant. Thus, both  $j_{-0.3}/j_{+0.3}$  V and  $j_{-0.5}/j_{+0.3}$  V can serve as ratiometric results for  $\text{H}_2\text{O}_2$  sensing [85].

Additionally, extra electroactive molecules can be introduced into the COFs-based EC system to accomplish the ratiometric analysis. For example, ferrocene (Fc) dicarboxylic acid molecules were directly introduced into the synthetic process of  $\text{COF}_{\text{ETTA-TPA}}$  nanospheres. The enwrapped Fc molecules not only increased the interlayer distance of  $\text{COF}_{\text{ETTA-TPA}}$  but also promoted the self-disproportionation of  $\text{H}_2\text{O}_2$ . Then, the produced  $\text{O}_2$  was electro-reduced by  $\text{COF}_{\text{ETTA-TPA}}$  at -0.5 V. Meanwhile, the reduction response at +0.45 V assigned to Fc molecules lowered with the



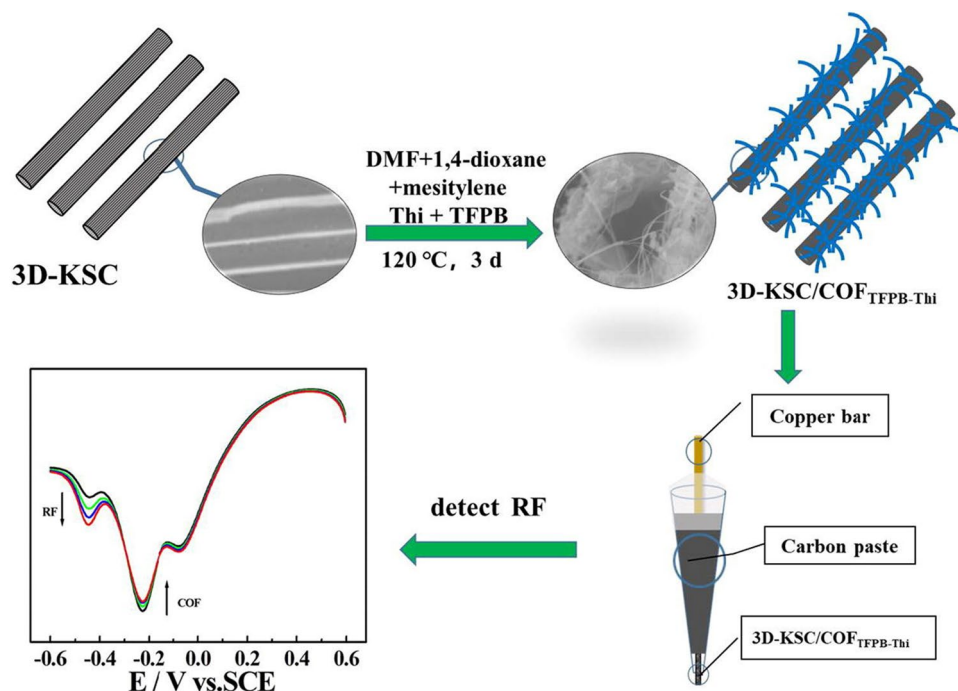


**Fig. 7** The synthesis process of 3D-KSC/COF<sub>Thi-TFPB</sub> and the fabrication of carbon paste electrode for ratiometric EC sensing of RF. Reproduced with permission from Ref. [84]. Copyright (2022) Elsevier

increasing dosage of  $\text{H}_2\text{O}_2$ . Thus, an “on–off” nonenzymatic ratiometric EC platform enabled the  $\text{H}_2\text{O}_2$  detection, showing a high sensitivity of  $0.009 \mu\text{M}^{-1}$  and a low LOD of  $0.33 \mu\text{M}$  [13]. Pang et al. electrodeposited AgNPs on a flexible carbon cloth and drop-coated COF-LZU1, which was prepared via the aminaldehyde condensation between PDA and TFB. Based on this, a stable EC response derived from AgNPs served as a standard signal, and COF-LZU1 enriched the targets, affording sensitive ratiometric responses toward bisphenol A (BPA) and bisphenol S (BPS) with a same LOD of  $0.15 \mu\text{M}$  [86].

### 3.2 Ions Sensors

Accurate and selective ions sensing is of great importance in both environmental and biological fields [20, 116]. Given the different electro-redox properties of heavy metal ions (HMIs), anodic stripping voltammetry (ASV) is attractive for HMIs sensing because of its high sensitivity, simplicity, rapidity, and ease of online monitoring [52, 53]. Although ASV can play to its strengths, common problems such as poor stability and scarce identification elements still limit the detection of trace HMIs. By virtue of rich and

diversiform absorption sites, COFs have attracted increasing attention in decorating high-quality HMIs sensing surfaces. For example, COF<sub>TAPB-DMTP</sub>, together with graphite powder and paraffin oil, was applied to manufacture carbon paste electrodes as ECL sensors, which achieved a remarkable current response to  $\text{Pb}^{2+}$  [52]. In another work, the sensitivity toward  $\text{Pb}^{2+}$  was significantly improved by modifying a glassy carbon electrode with an in-situ electroplated bismuth film and the nanocomposite of melamine (MA)-based COFs/ $\text{Fe}_3\text{O}_4$  NPs [87].

The presence of COFs greatly enlarges the electroactive surface area, and these edge-terminal amino groups can serve as adsorption sites. However, marginal sites that rely on incomplete condensation of COFs are far from sufficient, while post-synthetic modifications with special functional groups can provide enough absorption sites. For instance, hydrosulphonyl functionalized COF (COF-SH) was synthesized via a solvothermal method with TAPB and Dva, followed by trithiocyanuric acid (TTC) post-modification. Using this COF-SH as the electrode substrate, abundant S and N sites accumulated HMIs, affording their sensitive EC quantification. The LODs were down to 0.3, 0.2, 0.2, and



1.1  $\mu\text{g L}^{-1}$  for  $\text{Cd}^{2+}$ ,  $\text{Pb}^{2+}$ ,  $\text{Cu}^{2+}$ , and  $\text{Hg}^{2+}$  detection, respectively [53].

Moreover, to avoid laborious and time-consuming post-processing, the N- or S-rich monomers of benzo [1,2-b:3,4-b':5,6-b''] trithiophene-2,5,8-tricarbaldehyde (BTT) and TTA were selected for building rod-like  $\text{COF}_{\text{TTA-BTT}}$  through one-step amine-aldehyde condensation.  $\text{COF}_{\text{TTA-BTT}}$  was further employed for sensitive EC sensing of  $\text{Hg}^{2+}$ , showing a low LOD of 0.18 nM due to its significant enrichment [88]. Also,  $\text{COF}_{\text{MELE-BTDD}}$  with multiple active sites (N–S–N, –C=N) was prepared for the HMIs measurement by amine-aldehyde condensation of 2,5,8-triamino-s-heptazine (MELE) and 4,4'-(benzo[c] [1, 2, 5] thiadiazole-4,7-diyl) dibenzaldehyde (BTDD) [89]. The same group also synthesized lamellar  $\text{COF}_{\text{MA-Tp}}$  using monomers of MA and Tp, and each unit displayed six adsorption sites (–C=N, – $\text{NH}_2$ , –C=O) for the selective capture of HMIs [90].

In order to increase the solubility of large-sized COFs, controlled assembly of  $\text{COF}_{\text{BTLp-1}}$  on 3D-MC derived from kenaf stem was achieved by directly introducing 3D-MC into the amine-aldehyde polymerization process between 1,4-benzenedithiol-2,5-diamino-hydrochloride (BDDH) and TFB. The resultant  $\text{COF}_{\text{BTLp-1}}/3\text{D-MC}$  composite contained regular transport channels and twelve adsorption sites for both the transfer and adsorption of HMIs, which was further exploited for simultaneous detection of HMIs [24]. Besides,  $\text{COF}_{\text{TAPB-DMTP}}$  was also selected for controllable growth on the surface of  $\text{TiO}_2\text{-NH}_2$  via Schiff-base condensation. The nanocomposite was successfully employed for the determination of  $\text{Mn}^{2+}$  in Chinese liquor, and the LOD was as low as 0.0283 nM [91].

### 3.3 Immunosensors

Immunosensors relying on the highly specific recognition between antibodies (Abs) and antigens are prominent tools for the effective measurement of biomarkers [21]. During the past decades, EC immunological detection has aroused considerable concern because of its high sensitivity, splendid selectivity, simple operation, rapid response, and low sample consumption [117]. Generally, sandwich-type immunosensing has been recognized as one of the most popular modes, which utilizes captured Abs for target identification and reporter Abs tagged with probes or triggers to indicate signal changes [20, 118]. Thus, signal labels are the

key points for signal stability and amplification. Using the spherical  $\text{COF}_{\text{TAPB-DMTP}}$  as a carrier to sequentially load AuNPs, Abs, and HRP, a COF-supported signal probe was formed for the sandwiched EC immunosensing of cardiac troponin I (cTnI), a reliable biomarker of acute myocardial infarction, with a low LOD of 1.7  $\text{pg mL}^{-1}$ . Here, due to the enzymatic capacity of HRP, hydroquinone (HQ) was oxidized to benzoquinone (BQ) in the presence of  $\text{H}_2\text{O}_2$ , and BQ was then electro-reduced to output the amplified EC signals [92]. Also,  $\text{COF-LZU1}$  was co-doped with AuNPs, Abs, and the electron mediator toluidine blue (TB) to behave as a signal probe. Further using polypyrrole-modified  $\text{TiO}_2$  NPs as the sensing substrate, a sandwich-type EC immunosensor realized the cTnI detection, exhibiting linearity ranging from 0.5  $\text{pg mL}^{-1}$  to 10.0  $\text{ng mL}^{-1}$  and a low LOD of 0.17  $\text{pg mL}^{-1}$  [93]. Moreover, a magnetic  $\text{COF}_{\text{BD-Tp}}$  carried methylene blue (MB) for signal amplification. Briefly, magnetic  $\text{COF}_{\text{BD-Tp}}$  was synthesized by encapsulating  $\text{Fe}_3\text{O}_4$  nanocrystals with an amorphous polyimine network through a Schiff-base reaction, which was further manipulated into crystalline imine-linked COFs under thermodynamic control. Through multi-noncovalent interactions, abundant MB molecules were incorporated into the macrocyclic supramolecular hosts of  $\text{COF}_{\text{BD-Tp}}$ . Hence, using black phosphorene as a highly conductive matrix and this magnetic COFs-based probe for signal amplification, a sandwiched EC immunoassay realized the sensitive measurement of prostate specific antigen (PSA), an available serum biomarker of prostate tumors. The fabricated sensor achieved high analytical performance with a low LOD of 30  $\text{fg mL}^{-1}$  (Fig. 8A) [94].

Another significant issue is to create a highly conductive, catalytic, and reusable sensing interface. The intrinsic properties of COFs make them favorable as an emerging class of electrode matrixes for supporting substances. In particular, 2D COFs with periodic layered arrays of  $\pi$  clouds can promote charge/carrier transport. For example, Liu et al. demonstrated the use of PtNPs-decorated  $\text{COF-LZU1}$  as an EC platform for immunoassay. Meanwhile, AuNPs/MOFs (HKUST-1) complexes containing massive  $\text{Cu}^{2+}$  ions served as EC probes to show the expression of C-reactive protein (CRP), an effective indicator of infection, with a low LOD of 0.2  $\text{ng mL}^{-1}$  [95]. Besides, Boyacıoğlu et al. fabricated a sandwich-typed EC immunosensor for kidney injury molecule-1 (kim-1) detection based on AuNPs/ $\text{COF}_{\text{TAPB-TPA}}$  as the electrode substrate and  $\text{NiCo}_2\text{S}_4@\text{CeO}_2$  microspheres as the signal amplification tags. The prepared immunosensor

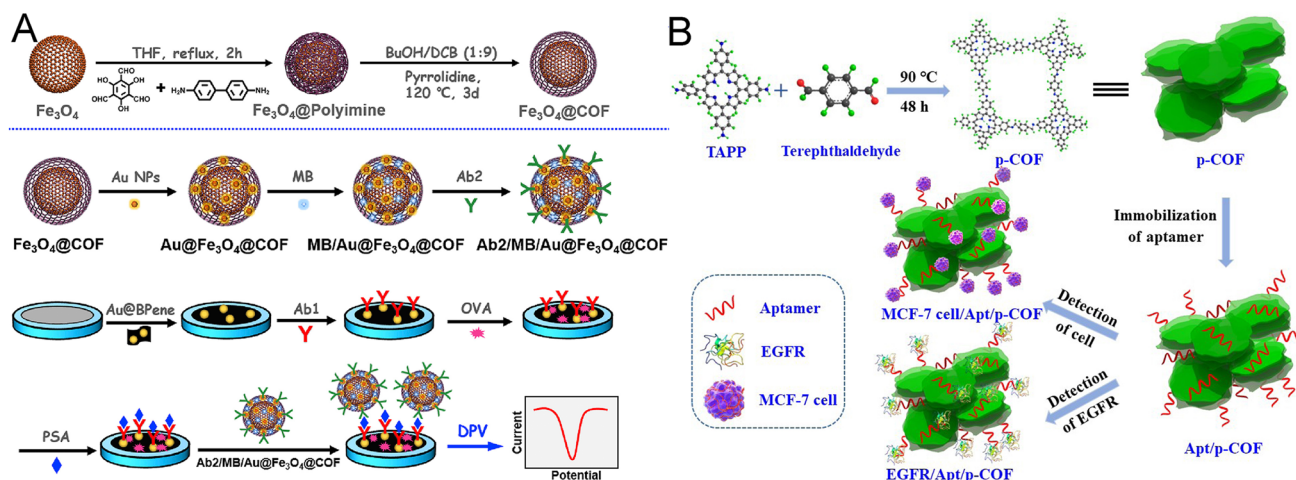


**Fig. 8** Schematic illustrations of **A** the preparation of  $\text{Fe}_3\text{O}_4@\text{COF}_{\text{BD-TP}}$  and the construction of an EC immunosensor for PSA detection, and **B** the synthesis of  $\text{COF}_{\text{TAPP-TPA}}$  and the fabrication of an EC aptasensor for MCF-7 cells and EGFR sensing. Reproduced with permission from Refs. [94, 104] Copyright (2019) Elsevier

exhibited good specificity, desirable stability, and acceptable reproducibility with a LOD down to  $2.00 \text{ fg mL}^{-1}$  [96]. Chen et al. developed a signal on–off ratiometric EC immunosensor to detect Amyloid- $\beta$  oligomer ( $\text{A}\beta\text{O}$ ), a reliable biomarker for the early diagnosis of Alzheimer’s disease. In this work, ultrasmall CuS NPs-loaded  $\text{COF}_{\text{TAPB-DMTP}}$  acted as the electrode substrate to catalyze HQ oxidation for detectable signals. At the same time, electroactive Thi-decorated AuNPs served as another EC signal label. After  $\text{A}\beta\text{O}$  was introduced, the HQ signal decreased while the Thi signal increased, resulting in the ratios for the accurate  $\text{A}\beta\text{O}$  evaluation with a low LOD of  $0.4 \text{ pM}$  [97].

### 3.4 Aptasensors

Aptamers represent synthetic single-stranded DNA or RNA oligonucleotides with unique 3D configurations, which can non-covalently bind to target molecules specifically [119, 120]. Aptasensors have been excitingly exploited by virtue of the advantages of aptamers, such as easy synthesis, low cost, good stability, and specific recognition ability. It is worth noting that the attributes of COFs guarantee the high loading capacity of aptamers via multiple interaction forces, thus establishing effective EC aptasensing platforms [46].

Similar to the sandwich-type immunosensor, a “peptide-target-aptamer” EC biosensor was constructed for norovirus detection based on  $\text{Au}@\text{black phosphorous NSs}@\text{COF}$

$\text{Ti}_3\text{C}_2\text{-MXene}$  nanohybrids as the electrode substance and  $\text{Au}@\text{ZnFe}_2\text{O}_4@\text{COF}_{\text{TAPB-TPA}}$  as the magnetic tag. The redox probe TB can be further linked to the magnetic tags to output an increased EC signal. Thus, the biosensor achieved desirable selectivity, anti-interference, and stability with a low LOD of  $0.003 \text{ copies mL}^{-1}$ , and it was successfully utilized for norovirus detection in stool samples without complex pretreatment [98]. Moreover, aptasensor can directly utilize the high-impedance target biomass to hinder the electron and mass transfer, thereby causing the decreased EC signals in a non-label manner. For example, Chen and his colleagues prepared the  $\text{AuNPs}@\text{Ce-COF}_{\text{Bpy-Tp}}$  (Bpy: 2,2'-bipyridine-5,5'-diamine) nanocomposite as the electrode matrix for aptamer immobilization. The sensors achieved the signal-off determination of zearalenone (ZEN) toxin, showing a low LOD of  $0.389 \text{ pg mL}^{-1}$  and a recovery in the range of 93.0–104.7% [99]. In another work, Song et al. synthesized  $\text{Fc-based COF}_{\text{HHTP-BFc}}$  by connecting 2,3,6,7,10,11-hexahydroxytriphenylene (HHTP) and 1,1'-ferrocenediboronic acid (BFc) via boronate esters linkages, and its Fc moiety displayed remarkable voltammetric response. Then, a signal-on aptasensing strategy allowed for the label-free cTnI detection, because the affinity between cTnI and the specific aptamers drove away the aptamers from the  $\text{COF}_{\text{HHTP-BFc}}$  surface, recovering its EC response [100].

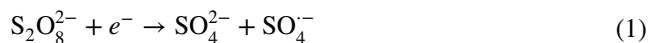
Electrochemical impedance spectroscopy (EIS), a simple, sensitive, label-free, and rapid method, has been widely used to collect signals generated by binding the analyte to

the specific aptamer-functionalized transducer interface. For example, Zhu et al. prepared  $\text{COF}_{\text{TAPB-DMTP}}/\text{AuNPs}$  and  $\text{COF}_{\text{TAPB-DMTP}}/\text{CNTs}$  as the covered substrates, which had a strong non-covalent affinity toward the aptamers of ciprofloxacin (CIP) and atrazine. Then, two EIS aptasensor achieved the detection of CIP and atrazine, showing low LODs of 7.06 fM and 3.11 pM, respectively [101, 102]. Wang et al. prepared an imine-linked  $\text{COF}_{\text{MA-TFPPy}}$  by polycondensation of MA and TFPPy.  $\text{COF}_{\text{MA-TFPPy}}$  showed strong immobilization of aptamers and fast charge-carrier mobility because of its high specific surface area, large pore cavities, rich surface groups, and extended  $\pi$ -conjugated frameworks. As such, a  $\text{COF}_{\text{MA-TFPPy}}$ -based EIS aptasensor allowed for sensitive determination of antibiotics, ampicillin (AMP) and ENR, yielding extremely low LODs of  $0.04 \text{ fg mL}^{-1}$  and  $6.07 \text{ fg mL}^{-1}$ , respectively [103]. This group also synthesized 2D porphyrin-based  $\text{COF}_{\text{TAPP-TPA}}$ . The highly conjugated NSs structure not only possessed improved EC activity but also facilitated the attachment of aptamers and biomolecules. The  $\text{COF}_{\text{TAPP-TPA}}$ -based aptasensor displayed remarkable analytical performance for living Michigan Cancer Foundation-7 (MCF-7) cells and epidermal growth factor receptor (EGFR) (Fig. 8B) [104]. In addition, a novel nanoarchitecture of Co-MOF@ $\text{COF}_{\text{CTF-1}}$  was synthesized by directly introducing the as-prepared  $\text{COF}_{\text{CTF-1}}$  into the Co-MOF synthesis process. This multi-layered Co-MOF@ $\text{COF}_{\text{CTF-1}}$  was used for EIS detection of AMP, one of the most frequently used  $\beta$ -lactam antibiotics, with an ultra-low LOD of  $0.217 \text{ fg mL}^{-1}$  [56].

## 4 COFs in ECL Sensing

A surge of interest in COFs has emerged in the ECL realm, but ECL research on COFs is still in its infancy. The coreactant ECL mechanism describes an electro-triggered luminescence with the assistance of appropriate coreactants, which is the most common route because of its high efficiency and easy implementation. Taking the example of potassium persulfate ( $\text{K}_2\text{S}_2\text{O}_8$ ), a representative “reduction–oxidation” coreactant for ECL-active COFs, the ECL emitting route is described as the Reactions 1–4. Briefly,  $\text{S}_2\text{O}_8^{2-}$  is electro-reduced to produce the strong oxidant radical intermediate  $\text{SO}_4^{\cdot-}$ . Meanwhile, ECL-active COFs undergo electro-reduction to form  $\text{COFs}^{\cdot-}$ . As a result, the radiative recombination of  $\text{SO}_4^{\cdot-}$  and  $\text{COFs}^{\cdot-}$  generates high-energy  $\text{COFs}^*$  to output

ECL. To achieve high analytical sensitivity of ECL sensors, developing efficient ECL emitters and designing nanomaterials-based amplification strategies are the two main ways [31, 121–125], both of which can be realized by COFs.



Unlike MOFs with metal nodes that might extinguish the ECL [126–128], metal-free COFs seem to be more suitable as ECL luminophores [125, 129]. Likewise, their general properties, such as high specific surface area and porous structure, guarantee high loading capacity and easy mass transport. As such, COFs can be activated with strong ECL emission by constructing intra-reticular charge transfer (IRCT) using non-ECL active monomers [59, 129]. At the same time, the rigid framework can restrict the intramolecular rotations and vibrations of luminogens to achieve aggregation-induced emission (AIE) effects [130]. Additionally, pore confinement and enrichment of COFs are also exploited as reliable substrates for special and sensitive ECL sensing applications [57, 131]. Therefore, COFs show great potential for designing next-generation ECL sensing devices. In this section, the reported COFs used in the ECL field will be discussed as ECL and non-ECL active ones.

### 4.1 ECL Active COFs

ECL depends on the charge transfer between luminophores and co-reactive groups or molecules [20, 132]. Thus, designing functional blocks to modulate the charge-transfer behaviors of the long-range ordered COFs can activate effective ECL emission. It is a promising approach to achieve efficient IRCT by integrating electron-donor and acceptor units into a reticular skeleton via topology-templated conjugation. For example, Luo et al. designed a type of donor–acceptor (D–A) COFs with triazine and triphenylamine motifs as strong ECL emitters. A control COF with slight D–A contrast was also prepared by replacing the triazine units with analogous benzene ones. By comparison, the optimal D–A

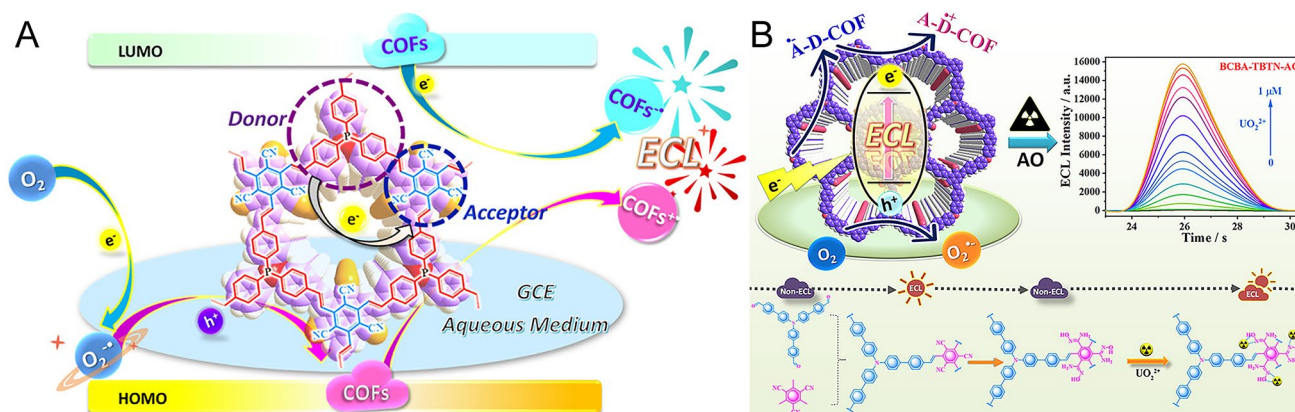


**Fig. 9** **A** Mechanism diagram of D-A fully conjugated COFs outputting ECL via IRCT. Reproduced with permission from Ref. [133]. Copyright (2021) American Chemical Society. **B** Schematic illustrations of the synthesis route for COF<sub>TBTN-BCBA</sub> and the ECL sensing application for  $UO_2^{2+}$ . Reproduced with permission from Ref. [134]. Copyright (2021) American Chemical Society

COF regulated by strong IRCT displayed a 123-fold increase in ECL. Experiments and density functional theory (DFT) calculations confirmed that the ECL behaviors were related to the crystallinity and protonation of the COFs, indicating the presence of IRCT between the D–A units. Further, the IRCT-mediated competitive oxidation mechanism afforded the decoding of the dual-peak ECL pattern of this D–A COF [129]. In another work, Qiu's group reported a general strategy for assembling a series of olefin-linked D–A COFs as ECL emitters. These D–A COFs are composed of two key acceptor subunits of 2,4,6-trimethyl-1,3,5-triazine (TMT) and 2,4,6-trimethylpyridine-3,5-dicarbonitrile (DCTP) with  $C_{3v}$  and  $C_{2v}$  symmetry, respectively, exhibiting different ECL responses. Through increasing chain length and blocks conjugation, the ECL efficiency was boosted. Further, efficient IRCT allowed robust ECL output without the need for exogenous toxic coreactants [59]. Following this work, the same group also investigated highly aligned D–A COFs with olefin linkages by co-crystallizing four electron-rich molecules (i.e., benzaldehyde, 4,4',4''-phosphinidynetris (BAP), 2,4,6-tris(4-formylphenyl)-1,3,5-triazine (TAPT), TFPB, and tris(4-formylphenyl)amine (TFPA)) and two electron-deficient molecules (i.e., TMT and 2,4,6-trimethylbenzene-1,3,5-tricarbonitrile (TBTN)) separately. Among these COFs, a tunable ECL was activated, and COF<sub>BAP-TBTN</sub> displayed the maximum ECL efficiency ( $\Phi_{ECL}$ ) of 32.1% in an aqueous solution with the coreactant of dissolved oxygen ( $O_2$ ). Quantum-chemical calculations suggested that the outstanding ECL performance was attributed to the reduced band gap and the good overlap of carriers within

the excited COFs (Fig. 9A) [133]. Soon after, this group also regulated IRCT within two other olefin-linked COFs, assembled with an acceptor of TBTN and two donors of 4-[4-[3,5-bis[4-(4-formylphenyl)-phenyl]phenyl]phenyl]benzoic acid (DAFB) and 4-[4-[4-(4-formylphenyl)-N-[4-(4-formylphenyl)phenyl]anilino]phenyl]-benzaldehyde (BCBA), respectively. In a similar manner, the D-A couples-powered IRCT aroused the ECL emitting out of these non-ECL active monomers. With endogenous  $O_2$  as the coreactant, COF<sub>TBTN-BCBA</sub> achieved prominent  $\Phi_{ECL}$  of 63.7% in a water medium, which was further employed for accurate ECL monitoring of  $UO_2^{2+}$  with a proportionable ECL increase (Fig. 9B) [134]. Following similar design concepts, in addition, this group also synthesized a class of ECL available COFs by conjugating BTT as a key electron donor and three electron receptors of TBTN, DCTP, and TMT via C=C bonding [130].

AIE refers to the fact that a material emits intense luminescence in the aggregated state, but no or weak light in the solution state [135, 136]. Developing AIE emitters is meaningful because ECL luminophores in practical use are usually randomly aggregated on the electrode surface and easily cause ECL quenching [135–137]. As it is, the rigid skeleton of COFs can restrict intramolecular vibrations and rotations of the AIE luminogens via intralayer covalent bonds and interlayer non-covalent  $\pi$ -interactions, resulting in reduced nonradiative transitions and the enhanced AIE effects. For example, an AIE unit, 4,4',4'',4'''-(ethene-1,1,2,2-tetrayl) tetrabenzaldehyde (ETB), was utilized as a key monomer to prepare three olefin-linked COFs. These COFs exhibited



predominant framework-induced ECL in aqueous solution, far exceeding those of monomeric aggregated states, because the ordered framework not only promoted efficient charge transfer for an excited-state generation but also reduced the ETB rotation-caused nonradiative loss [138]. Li et al. designed an AIE-COF by a Schiff base reaction between TAPT and 4,4'-diamino-2,2'-bipyridine (DB), appearing to an excellent ECL performance in the presence of  $\text{H}_2\text{O}_2$ . Further coupled with  $\text{Co}_3\text{O}_4$  nanozyme for amplifying the signal, a molecularly imprinted polymer (MIP) ECL biosensor was constructed for antibiotic chloramphenicol testing with a LOD of 0.118 pM [139]. In another work, [(1,3,5-triazine-2,4,6-triyl)tris(benzene-4,1-diyl)]triboronic acid (TTBT) was used to design an AIE-COF material via boric acid dehydration condensation, which was further employed for the construction of a MIP ECL biosensor [140]. Zhang et al. synthesized pyrene-based  $sp^2$  carbon-conjugated COF NSs by C=C polycondensation between 2,2'-(1,4-phenylene) diacetonitrile (PDAN) and TFPPy. In this structure, the AIE-luminogens of cyano-substituted phenylenevinylene and the pyrene luminophores were topologically connected together to reduce the aggregation-caused quenching effect. Further using  $\text{Bu}_4\text{NPF}_6$  as the coreaction accelerator of the COF NSs/ $\text{S}_2\text{O}_8^{2-}$  ECL system, an ECL genosensor enabled the microRNA-21 detection with a low LOD of 46 aM via three cascaded Exo III-mediated recycling processes for signal amplification [141].

Although COFs have a high assembling capacity for ECL phosphors or motifs, the intrinsic poor conductivity still limits the ECL performance (generally  $< 10^{-8} \text{ S m}^{-1}$ ). To address this issue, Zhang et al. designed a conductive COF with a fully  $\pi$ -conjugated planar structure by connecting HHTP and 2,3,6,7,10,11-hexaaminotriphenylene (HATP) via pyrazine linkages. The splendid ECL emission was achieved as a result of the superior electronic conductivity ( $3.11 \times 10^{-4} \text{ S m}^{-1}$ ), the luminophores directly as building blocks, and the porous structure that allows free diffusion of electrolyte. Based on  $\text{COF}_{\text{HHTP-HATP}}$  after pre-reduction electrolysis in  $\text{S}_2\text{O}_8^{2-}$  solution as an efficient solid-state ECL material, an “off-on” ECL platform was established for sensitive determination of thrombin through aptamer/target proximity binding-mediated 3D bipedal DNA walker for signal amplification [58]. Cui et al. prepared a fully- $\pi$  conjugated  $\text{COF}_{\text{DMTP-TCPB}}$  with  $sp^2$  carbon-linkage via Knoevenagel polycondensation of DMTP and

1,3,5-tris(4-cynomethylphenyl)benzene (TCPB), exhibiting high ECL efficiency for alkaline phosphatase detection [142].

Additionally, various ECL-active COFs are springing up, accompanying their ECL sensing applications. For instance, Yang et al. designed a stable Ru-complex-based metal-COF using a classic ECL luminophore, tris(4,4'-dicarboxylicacid-2,2'-bipyridyl)ruthenium(II) ( $\text{Ru}(\text{dcbpy})_3^{2+}$ ), as a building motif. Owing to the topologically ordered and porous architectures, this Ru-MOF displayed strong ECL emitting and remarkable chemical stability for the microRNA-155 detection, achieving an ultralow LOD of 3.02 aM [143]. Song et al. demonstrated the synthesis of an aminated-linked COF using the luminescent monomers tetraphenylethylene (TPE) derivative and piperazine, which was further utilized to establish an ECL platform to selectively discriminate enantiomer of phenylalanine [144]. The same group also exploited this aminated-linked COF for glutathione (GSH) ECL assay with a LOD of 17 nM. In this work, target GSH can reduce the quencher of  $\text{MnO}_2$  NSs into  $\text{Mn}^{2+}$ , restoring the ECL emission accordingly [145]. Lately, Qiu's group designed structural isomerism of COFs with different ECL effects, which were further employed for the sensitive toxic As(V) detection with an ultralow LOD of 0.33 nM [146]. This group also constructed a COF-based host-guest system by guest molecular assembly with strong ECL emission and realized the nuclear contamination analysis of  $\text{UO}_2^{2+}$  [147]. Besides, ECL potential tunable COFs are realized by changing the electron and spatial in the precursor, and the generated COF skeleton with reduced potential and increased ECL intensity was used for the selective ECL detection of lutetium ion, showing a LOD as low as 1.6 nM [148].

## 4.2 Non-ECL Active COFs

In addition to being directly used as ECL emitters, COFs can also be made into microreactors to accumulate luminophores and coreactants, thus boosting ECL efficiency due to the confinement effect. For example, Zeng et al. loaded tris(2,2'-bipyridyl) ruthenium(II) ( $\text{Ru}(\text{bpy})_3^{2+}$ ) onto  $\text{COF-LZU1}$ , displaying increased nearly fivefold ECL intensity with a standard of classical  $\text{Ru}(\text{bpy})_3^{2+}$ /tripropylamine (TPrA) system. In this work,  $\text{COF-LZU1}$  can not only load massive  $\text{Ru}(\text{bpy})_3^{2+}$  but also enrich a large amount of TPrA from the solution via the hydrophobic interaction. Thus, using



COF-LZU1 as an ECL microreactor, a confined microenvironment was well created for the redox and survival of coreactants. Through Nt. BbvCI restriction endonuclease-powered DNA walker and T7 exonuclease-mediated target recycling for dual signal amplification, these microreactors were further employed for ultrasensitive ECL detection of aflatoxin M1, showing a low LOD of  $0.009 \text{ pg mL}^{-1}$  [131].

Microporous COFs can act as efficient adsorbents for small organic molecules due to the electrostatic, hydrophobic, hydrogen bonding, and  $\pi$ - $\pi$  interactions [9, 57]. Thus, the presence of COFs can enrich target analytes and improve analytical behaviors. Our group designed a biomimetic hollow organic nanosphere by orderly hybridizing imine-linked COFs with hollow  $\text{g-C}_3\text{N}_4$  nanosphere (Fig. 10). On the basis of the quenching effect of tetracycline (Tc) on the  $\text{g-C}_3\text{N}_4/\text{O}_2$  ECL system, these bioinspired nanospheres served as nanoprobe for ultrasensitive detection of Tc, and the LOD achieved a sub-part per billion level of  $0.031 \text{ } \mu\text{g L}^{-1}$ . Experiments and theoretical derivation demonstrated that COF shells played an important role in enriching Tc, and the target amount is equivalent to being amplified around  $\text{g-C}_3\text{N}_4$  accordingly. Besides, the Tc quencher and the coreactant radicals traveled and mutually reacted within the narrow and long nanopore channels, ensuring again high quenching effect. Furthermore, a novel ECL technology utilizing the biomimetic self-responsiveness of these nanoprobe realized the evaluation of the photodegradation process [57].

In addition, COFs with high specific surface area and porosity can also serve as excellent electrode matrixes to support catalytic centers in a well-dispersed manner for amplified ECL outputs. For example, a liquid-liquid interface assembly strategy allowed for the polymerization of Zr-coordinated amide porphyrin-based COFs. This Zr-porphyrin-based COF adopted a 2D multilayer structure with high conductivity and electrocatalysis performance toward the luminol/ $\text{H}_2\text{O}_2$  ECL system, which was further utilized to construct a novel MIP ECL sensor for Tc detection based on the gate control effect [149]. Li and co-workers exploited  $\text{COF}_{\text{TAPB-Dva}}$  as a carrier to load abundant Au nanoclusters for  $\text{Pb}^{2+}$  ECL sensing. In comparison with solid-state aggregated Au nanoclusters, the COF-confined ones displayed a 3.3-fold enhancement in anodic ECL efficiency. As such, the fabricated ECL biosensor obtained sensitive detection of  $\text{Pb}^{2+}$  down to  $7.9 \text{ pM}$  [150]. Ma et al. prepared a carbon dots (CDs)-based COF via the condensation reaction of aldehyde-CDs and TAPB, leading to the regular arrangement of

CDs with efficient ECL emission in the presence of  $\text{K}_2\text{S}_2\text{O}_8$  and  $\text{Bu}_4\text{NPF}_6$ . Further combined with a CRISPR/Cas12a trans-cutting strategy, a high-performance ECL biosensor realized the BPA sensing with a LOD as low as  $2.21 \text{ fM}$  [151]. Besides, *N*-(4-aminobutyl)-*N*-ethylisoluminol (ABEI) was also linked to COF-LZU1 as an ECL emitter for label-free signal-off detection of cytochrome c. This sensor exhibited a wide linear range of  $1.00 \text{ fg mL}^{-1}$ – $0.10 \text{ ng mL}^{-1}$  and a low LOD down to  $0.73 \text{ fg mL}^{-1}$  [152].

## 5 Conclusions and Perspective

This review primarily provides an overview of the state-of-the-art COFs utilized in the field of electroanalytical chemistry, sketching the trajectory from basic characteristics and general synthesis strategies to the resultant sensing usages. The progress of elaborate COFs-based EC sensors is discussed systematically, including ions sensors, chemical sensors, immunosensors, and aptasensors. These COFs-based EC sensors demonstrated superior analytical performance. (1) Until now, imine-linked COFs formed by aminaldehyde condensation remain the most reported COFs for EC sensing applications due to their facile synthesis, high crystallinity, and stability. (2) Their high specific surface area provides a large electrode active area and high loading capacity, and the super-micropores and ordered channels ensure favorable energy/mass transfer. (3) Nano-sized pores and existing heteroatoms can trap guest targets through non-covalent interactions. (4) COFs generally exhibit flexibility, good biocompatibility, low toxicity, and high stability, beneficial for the fabrication of repeatable and reproducible EC sensors. (5) Framework networks designed by  $\pi$ -stacked or extended  $\pi$ -conjugated backbones, for example, that are COFs via pyrazine or olefin linkage, possess acceptable electrical conductivity. (6) Ratiometric EC sensing can be executed for accurate results based on the unique electroactive COFs.

In addition, ECL available COFs and their preliminary sensing applications are summarized in detail. (1) At present, modulating the IRCT behavior of COFs is a common strategy to activate ECL from non-ECL active monomers. (2) AIE-ECL COFs can be facilely achieved because the rigid framework restricts the intramolecular rotations and vibrations of luminogens. (3) Designing COFs with a fully  $\pi$ -conjugated planar structure can improve the conductivity and achieve fast charge injection. (4) The inherent



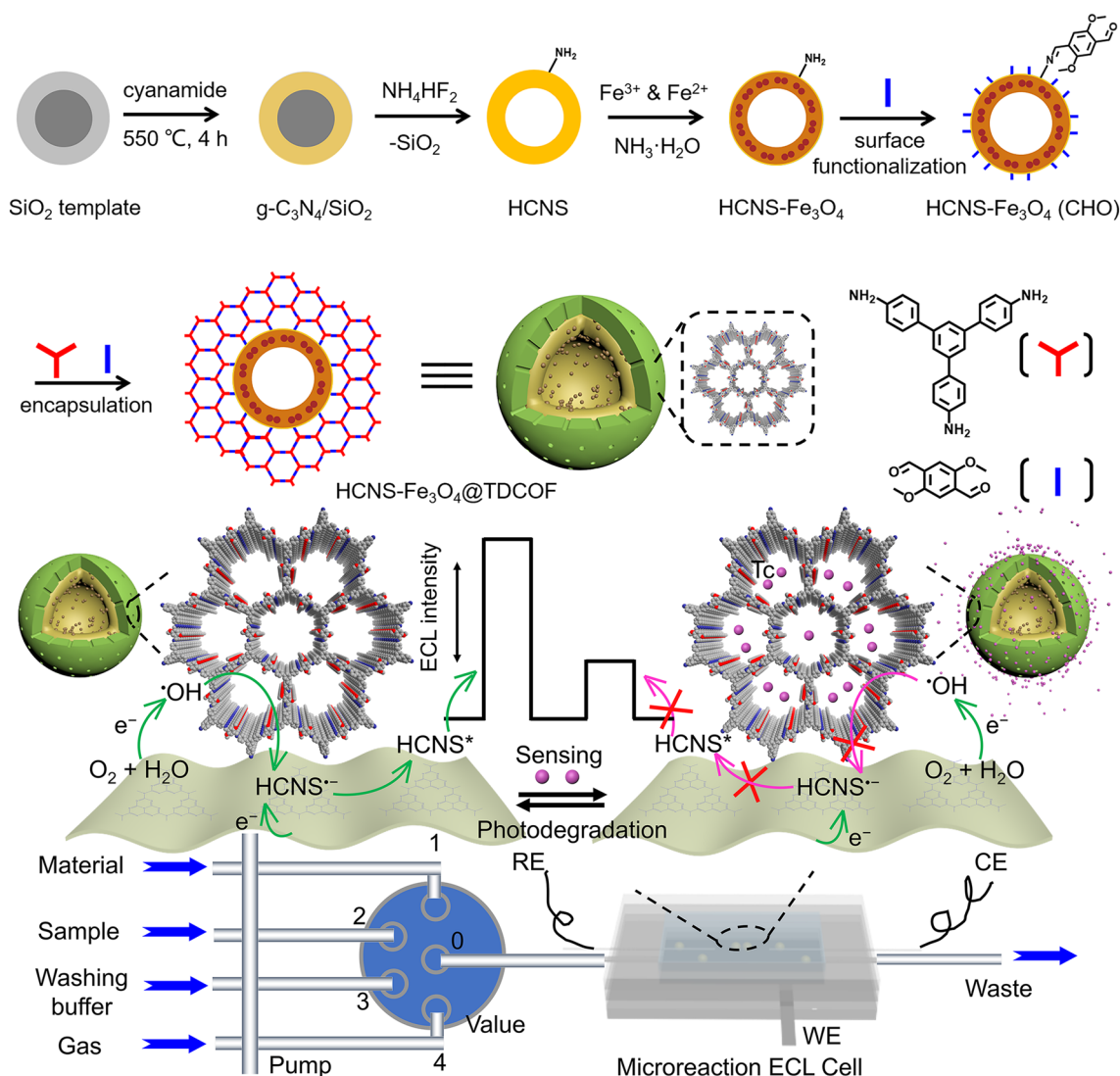


**Fig. 10** Schematic illustrations of the preparation progress of a biomimetic hollow organic crystalline nanosphere and the instrument and principle for Tc sensing. Reproduced with permission from Ref. [57]. Copyright (2022) Wiley–VCH

characteristics of non-ECL active COFs make them the right microreactors, strong absorbents, and electrode matrices with high specific surface area, thereby improving the performance of ECL sensors.

Therefore, we believe that COFs are capable of taking a place in the field of electroanalytical chemistry, accompanied by the development of advanced synthetic methods and the disclosure of unique attributes in future work. Despite impressive progress, various obstacles remain to be addressed for the wide applications of COFs in electroanalytical chemistry. First, the solvothermal method still dominates the COFs preparation, but it usually requires

tedious synthesis procedures and harsh reaction conditions. Second, COFs composed of non-conductive organic motifs are severely restricted as electroactive substances for EC sensing. The synthesis of highly conductive COFs is still relatively challenging work. Third, due to poor affinity, the assembly of COFs at the interface makes it difficult to achieve high efficiency and reproducibility. Most of the current works focus on the direct use of COFs while ignoring the vital role of modification strategies. Fourth, theoretical prediction of the covalent ordered structure of COFs and their EC behaviors is an arduous task. Lastly, the potential

biotoxicity of COFs may affect their further commercial applications.

A few shallow outlooks are only for the reference of readers. In terms of the EC sensing aspect, it is a promising direction to develop conductive COFs with completely  $\pi$ -conjugated planar structures. Assembling COFs-derived composites with particular architecture can also access good conductivity and affinity. Usually, COFs prepared through the traditional solvothermal method exhibit nonuniform bulky morphology, so it is meaningful to develop synthetic strategies for special structures, such as hollow nanostructures mimicking containers, vesicles, and cells. Certainly, developing facile, green, and mild synthetic methods is a must for the large-scale manufacture of COFs-based EC sensors. Pre-functionalized monomers or post-synthetic modifications to exploit the diversity of species and functions of COFs have great potential for future development. Furthermore, most reported COFs possess only micropores, preventing guests (e.g., enzymes, quantum dots) from entering the active cavities or open channels, and creating hierarchical porosity in crystal COFs is highly desired accordingly. In particular, the *in-situ* interface assembly strategy of COFs awaits further exploration to establish stable and repeatable sensing platforms. In the ECL domain, although some ECL available COFs have been discovered, the ECL research on COFs is still in its initial stage. Future research is suggested to focus on the design of novel COFs emitters, the study of structure-related ECL behaviors, the dependence of their physicochemical properties and electronic structure on the ECL efficiency, the disclosure of underlying ECL reactions occurring in COFs, as well as expanding ECL assays.

**Acknowledgements** This research was supported by Natural Science Foundation of Jiangsu Province (BK20220405), National Natural Science Foundation of China (21834004, 22276100, 22304086), Key Laboratory for Organic Electronics & Information Displays, NJUPT (GZR2022010010, GZR2023010045), Nanjing Science and Technology Innovation Project for Chinese Scholars Studying Abroad (NJKCZYZZ2022-01), Research Fund for Jiangsu Distinguished Professor (RK030STP22001), Natural Science Research Start-up Foundation of Recruiting Talents of NJUPT (NY221006, NY223051), Natural Science Foundation of the Jiangsu Higher Education Institutions of China (23KJB150025), and State Key Laboratory of Analytical Chemistry for Life Science, Nanjing University (SKLACLS2311).

**Funding** Open access funding provided by Shanghai Jiao Tong University.

**Declarations**

**Conflict of interest** The authors declare no interest conflict. They have no known competing financial interests or personal relationships that could have appeared to influence the work reported in this paper.

**Open Access** This article is licensed under a Creative Commons Attribution 4.0 International License, which permits use, sharing, adaptation, distribution and reproduction in any medium or format, as long as you give appropriate credit to the original author(s) and the source, provide a link to the Creative Commons licence, and indicate if changes were made. The images or other third party material in this article are included in the article's Creative Commons licence, unless indicated otherwise in a credit line to the material. If material is not included in the article's Creative Commons licence and your intended use is not permitted by statutory regulation or exceeds the permitted use, you will need to obtain permission directly from the copyright holder. To view a copy of this licence, visit <http://creativecommons.org/licenses/by/4.0/>.

## References

1. A.P. Côté, A.I. Benin, N.W. Ockwig, M. O'Keeffe, A.J. Matzger et al., Porous, crystalline, covalent organic frameworks. *Science* **310**(5751), 1166–1170 (2005). <https://doi.org/10.1126/science.1120411>
2. K. Geng, T. He, R. Liu, S. Dalapati, K.T. Tan et al., Covalent organic frameworks: design, synthesis, and functions. *Chem. Rev.* **120**(16), 8814–8933 (2020). <https://doi.org/10.1021/acs.chemrev.9b00550>
3. N. Huang, P. Wang, D. Jiang, Covalent organic frameworks: a materials platform for structural and functional designs. *Nat. Rev. Mater.* **1**(10), 16068 (2016). <https://doi.org/10.1038/natrevmats.2016.68>
4. H. Xu, J. Gao, D. Jiang, Stable, crystalline, porous, covalent organic frameworks as a platform for chiral organocatalysts. *Nat. Chem.* **7**(11), 905–912 (2015). <https://doi.org/10.1038/nchem.2352>
5. Y. Jin, Y. Hu, W. Zhang, Tessellated multiporous two-dimensional covalent organic frameworks. *Nat. Rev. Chem.* **1**(7), 0056 (2017). <https://doi.org/10.1038/s41570-017-0056>
6. P. Pachfule, A. Acharjya, J. Roeser, T. Langenhahn, M. Schwarze et al., Diacetylene functionalized covalent organic framework (COF) for photocatalytic hydrogen generation. *J. Am. Chem. Soc.* **140**(4), 1423–1427 (2018). <https://doi.org/10.1021/jacs.7b11255>
7. Y. Xiong, Q. Liao, Z. Huang, X. Huang, C. Ke et al., Ultra-high responsivity photodetectors of 2D covalent organic frameworks integrated on graphene. *Adv. Mater.* **32**(9), 1907242 (2020). <https://doi.org/10.1002/adma.201907242>
8. E. Vitaku, C.N. Gannett, K.L. Carpenter, L. Shen, H.D. Abruña et al., Phenazine-based covalent organic framework cathode materials with high energy and power densities. *J. Am. Chem. Soc.* **142**(1), 16–20 (2020). <https://doi.org/10.1021/jacs.9b08147>



9. S. Karak, K. Dey, A. Torris, A. Halder, S. Bera et al., Inducing disorder in order: hierarchically porous covalent organic framework nanostructures for rapid removal of persistent organic pollutants. *J. Am. Chem. Soc.* **141**(18), 7572–7581 (2019). <https://doi.org/10.1021/jacs.9b02706>
10. Q.Q. Jiang, Y.J. Li, Q. Wu, R.P. Liang, X. Wang et al., Molecular insertion: a master key to unlock smart photoelectric responses of covalent organic frameworks. *Small* **19**, e2302254 (2023). <https://doi.org/10.1002/sml.202302254>
11. J. Chang, C. Li, X. Wang, D. Li, J. Zhang et al., Quasi-three-dimensional cyclotriphosphazene-based covalent organic framework nanosheet for efficient oxygen reduction. *Nano-Micro Lett.* **15**(1), 159 (2023). <https://doi.org/10.1007/s40820-023-01111-8>
12. E. Bakker, M. Telting-Diaz, Electrochemical sensors. *Anal. Chem.* **74**(12), 2781–2800 (2002). <https://doi.org/10.1021/ac0202278>
13. H. Liang, M. Xu, Y. Zhu, L. Wang, Y. Xie et al.,  $\text{H}_2\text{O}_2$  ratio-metric electrochemical sensors based on nanospheres derived from ferrocene-modified covalent organic frameworks. *ACS Appl. Nano Mater.* **3**(1), 555–562 (2019). <https://doi.org/10.1021/acsanm.9b02117>
14. H. Liang, L. Wang, Y. Yang, Y. Song, L. Wang, A novel biosensor based on multienzyme microcapsules constructed from covalent-organic framework. *Biosens. Bioelectron.* **193**, 113553 (2021). <https://doi.org/10.1016/j.bios.2021.113553>
15. N. Karimian, P. Hashemi, A. Afkhami, H. Bagheri, The principles of bipolar electrochemistry and its electroanalysis applications. *Curr. Opin. Electrochem.* **17**, 30–37 (2019). <https://doi.org/10.1016/j.coelec.2019.04.015>
16. A. Khanmohammadi, A. Jalili Ghazizadeh, P. Hashemi, A. Afkhami, F. Arduini et al., An overview to electrochemical biosensors and sensors for the detection of environmental contaminants. *J. Iran. Chem. Soc.* **17**(10), 2429–2447 (2020). <https://doi.org/10.1007/s13738-020-01940-z>
17. Y. Cao, J.J. Zhu, Recent progress in electrochemiluminescence of halide perovskites. *Front. Chem.* **9**, 629830 (2021). <https://doi.org/10.3389/fchem.2021.629830>
18. Y. Cao, Y. Zhou, Y. Lin, J.J. Zhu, Hierarchical metal-organic framework-confined  $\text{CsPbBr}_3$  quantum dots and aminated carbon dots: a new self-sustaining suprastructure for electrochemiluminescence bioanalysis. *Anal. Chem.* **93**(3), 1818–1825 (2021). <https://doi.org/10.1021/acs.analchem.0c04717>
19. T. Han, C. Ma, L. Wang, Y. Cao, H.Y. Chen et al., A novel electrochemiluminescence Janus emitter for dual-mode biosensing. *Adv. Funct. Mater.* **32**(24), 2200863 (2022). <https://doi.org/10.1002/adfm.202200863>
20. Y. Cao, J.L. Zhou, Y. Ma, Y. Zhou, J.J. Zhu, Recent progress of metal nanoclusters in electrochemiluminescence. *Dalton Trans.* **51**(23), 8927–8937 (2022). <https://doi.org/10.1039/d2dt00810f>
21. C. Ma, Y. Cao, X. Gou, J.J. Zhu, Recent progress in electrochemiluminescence sensing and imaging. *Anal. Chem.* **92**(1), 431–454 (2020). <https://doi.org/10.1021/acs.analchem.9b04947>
22. C. Zhang, M. Cui, J. Ren, Y. Xing, N. Li et al., Facile synthesis of novel spherical covalent organic frameworks integrated with Pt nanoparticles and multiwalled carbon nanotubes as electrochemical probe for tanshinol drug detection. *Chem. Eng. J.* **401**, 126025 (2020). <https://doi.org/10.1016/j.cej.2020.126025>
23. Y. Chen, Y. Xie, X. Sun, Y. Wang, Y. Wang, Tunable construction of crystalline and shape-tailored  $\text{Co}_3\text{O}_4$ @TAPB-DMTP-COF composites for the enhancement of tert-butylhydroquinone electrocatalysis. *Sens. Actuators B Chem.* **331**, 129438 (2021). <https://doi.org/10.1016/j.snb.2021.129438>
24. J. Han, J. Yu, Y. Guo, L. Wang, Y. Song, COFBTL $\text{P}^{\text{I}}$ /three-dimensional macroporous carbon electrode for simultaneous electrochemical detection of  $\text{Cd}^{2+}$ ,  $\text{Pb}^{2+}$ ,  $\text{Cu}^{2+}$  and  $\text{Hg}^{2+}$ . *Sens. Actuators B Chem.* **321**, 128498 (2020). <https://doi.org/10.1016/j.snb.2020.128498>
25. X.Y. Ji, K. Sun, Z.K. Liu, X. Liu, W. Dong et al., Identification of dynamic active sites among Cu species derived from MOFs@CuPc for electrocatalytic nitrate reduction reaction to ammonia. *Nano-Micro Lett.* **15**(1), 110 (2023). <https://doi.org/10.1007/s40820-023-01091-9>
26. N. Karimian, P. Hashemi, A. Khanmohammadi, A. Afkhami, H. Bagheri, The principles and recent applications of bioelectrocatalysis. *Anal. Bioanal. Chem. Res.* **7**(3), 281–301 (2020). <https://doi.org/10.22036/ABCR.2020.206676.1423>
27. M.M. Bordbar, A. Sheini, P. Hashemi, A. Hajian, H. Bagheri, Disposable paper-based biosensors for the point-of-care detection of hazardous contaminations-a review. *Biosensors* **11**(9), 316 (2021). <https://doi.org/10.3390/bios11090316>
28. Y. Gao, J. Wang, Y. Yang, J. Wang, C. Zhang et al., Engineering spin states of isolated copper species in a metal-organic framework improves urea electrosynthesis. *Nano-Micro Lett.* **15**(1), 158 (2023). <https://doi.org/10.1007/s40820-023-01127-0>
29. H. Fakhri, H. Bagheri, Highly efficient Zr-MOF@ $\text{WO}_3$ /graphene oxide photocatalyst: synthesis, characterization and photodegradation of tetracycline and malathion. *Mat. Sci. Semicon. Proc.* **107**, 104815 (2020). <https://doi.org/10.1016/j.mssp.2019.104815>
30. N. Karimian, H. Fakhri, S. Amidi, A. Hajian, F. Arduini et al., A novel sensing layer based on metal-organic framework UiO-66 modified with  $\text{TiO}_2$ -graphene oxide: application to rapid, sensitive and simultaneous determination of paraoxon and chlorpyrifos. *New J. Chem.* **43**(6), 2600–2609 (2019). <https://doi.org/10.1039/c8nj06208k>
31. S.M. Khoshfetrat, H. Khoshshafar, A. Afkhami, M.A. Mehrgardi, H. Bagheri, Enhanced visual wireless electrochemiluminescence immunosensing of prostate-specific antigen based on the luminol loaded into MIL-53(Fe)- $\text{NH}_2$  accelerator and hydrogen evolution reaction mediation. *Anal. Chem.* **91**(9), 6383–6390 (2019). <https://doi.org/10.1021/acs.analchem.9b01506>
32. H. Khoshshafar, N. Karimian, T.A. Nguyen, H. Fakhri, A. Khanmohammadi et al., Enzymeless voltammetric sensor for simultaneous determination of parathion and paraoxon based on Nd-based metal-organic framework. *Chemosphere*



- 292, 133440 (2022). <https://doi.org/10.1016/j.chemosphere.2021.133440>
33. B. Cao, H. Liu, X. Zhang, P. Zhang, Q. Zhu et al., MOF-derived ZnS nanodots/Ti<sub>3</sub>C<sub>2</sub>Tx mxene hybrids boosting superior lithium storage performance. *Nano-Micro Lett.* **13**(1), 202 (2021). <https://doi.org/10.1007/s40820-021-00728-x>
  34. Z. Ye, Y. Jiang, L. Li, F. Wu, R. Chen, Rational design of mof-based materials for next-generation rechargeable batteries. *Nano-Micro Lett.* **13**(1), 203 (2021). <https://doi.org/10.1007/s40820-021-00726-z>
  35. X. Huang, J. Wei, Y. Zhang, B. Qian, Q. Jia et al., Ultralight magnetic and dielectric aerogels achieved by metal-organic framework initiated gelation of graphene oxide for enhanced microwave absorption. *Nano-Micro Lett.* **14**(1), 107 (2022). <https://doi.org/10.1007/s40820-022-00851-3>
  36. G. Nagaraju, S.C. Sekhar, B. Ramulu, S.K. Hussain, D. Nar-simulu et al., Ternary MOF-based redox active sites enabled 3D-on-2D nanoarchitected battery-type electrodes for high-energy-density supercapacities. *Nano-Micro Lett.* **13**(1), 17 (2020). <https://doi.org/10.1007/s40820-020-00528-9>
  37. Z. Cao, R. Momen, S. Tao, D. Xiong, Z. Song et al., Metal-organic framework materials for electrochemical supercapacitors. *Nano-Micro Lett.* **14**(1), 181 (2022). <https://doi.org/10.1007/s40820-022-00910-9>
  38. J. Chen, D. Sheng, T. Ying, H. Zhao, J. Zhang et al., MoFs-based nitric oxide therapy for tendon regeneration. *Nano-Micro Lett.* **13**(1), 23 (2020). <https://doi.org/10.1007/s40820-020-00542-x>
  39. X. He, Fundamental perspectives on the electrochemical water applications of metal-organic frameworks. *Nano-Micro Lett.* **15**(1), 148 (2023). <https://doi.org/10.1007/s40820-023-01124-3>
  40. Y. Hu, H. Huang, D. Yu, X. Wang, L. Li et al., All-climate Aluminum-ion batteries based on binder-free mof-derived FeS<sub>2</sub>@C/CNT cathode. *Nano-Micro Lett.* **13**(1), 159 (2021). <https://doi.org/10.1007/s40820-021-00682-8>
  41. J. Huang, P. Wu, Controlled assembly of luminescent lanthanide-organic frameworks via post-treatment of 3D-printed objects. *Nano-Micro Lett.* **13**(1), 15 (2020). <https://doi.org/10.1007/s40820-020-00543-w>
  42. Y. Lu, R. Zhou, N. Wang, Y. Yang, Z. Zheng et al., Engineer nanoscale defects into selective channels: MOF-enhanced Li<sup>+</sup> separation by porous layered double hydroxide membrane. *Nano-Micro Lett.* **15**(1), 147 (2023). <https://doi.org/10.1007/s40820-023-01101-w>
  43. C. Li, Y. Ji, Y. Wang, C. Liu, Z. Chen et al., Applications of metal-organic frameworks and their derivatives in electrochemical CO<sub>2</sub> reduction. *Nano-Micro Lett.* **15**(1), 113 (2023). <https://doi.org/10.1007/s40820-023-01092-8>
  44. Y. Zhu, K. Yue, C. Xia, S. Zaman, H. Yang et al., Recent advances on MOF derivatives for non-noble metal oxygen electrocatalysts in zinc-air batteries. *Nano-Micro Lett.* **13**(1), 137 (2021). <https://doi.org/10.1007/s40820-021-00669-5>
  45. X. Chen, L. Kong, J.A. Mehrez, C. Fan, W. Quan et al., Outstanding humidity chemiresistors based on imine-linked covalent organic framework films for human respiration monitoring. *Nano-Micro Lett.* **15**(1), 149 (2023). <https://doi.org/10.1007/s40820-023-01107-4>
  46. R. Yuan, H.K. Li, H. He, Recent advances in metal/covalent organic framework-based electrochemical aptasensors for biosensing applications. *Dalton Trans.* **50**(40), 14091–14104 (2021). <https://doi.org/10.1039/d1dt02360h>
  47. X. Zhao, P. Pachfule, A. Thomas, Covalent organic frameworks (COFs) for electrochemical applications. *Chem. Soc. Rev.* **50**(12), 6871–6913 (2021). <https://doi.org/10.1039/d0cs01569e>
  48. X. Zhang, G. Li, D. Wu, B. Zhang, N. Hu et al., Recent advances in the construction of functionalized covalent organic frameworks and their applications to sensing. *Biosens. Bioelectron.* **145**, 111699 (2019). <https://doi.org/10.1016/j.bios.2019.111699>
  49. B. Mohan, R. Kumari, Virender, G. Singh, K. Singh et al., Covalent organic frameworks (COFs) and metal-organic frameworks (MOFs) as electrochemical sensors for the efficient detection of pharmaceutical residues. *Environ. Int.* **175**, 107928 (2023). <https://doi.org/10.1016/j.envint.2023.107928>
  50. X. Xu, Z. Zhang, R. Xiong, G. Lu, J. Zhang et al., Bending resistance covalent organic framework superlattice: “nano-hourglass”-induced charge accumulation for flexible in-plane micro-supercapacitors. *Nano-Micro Lett.* **15**(1), 25 (2022). <https://doi.org/10.1007/s40820-022-00997-0>
  51. G. Yan, X. Sun, Y. Zhang, H. Li, H. Huang et al., Metal-free 2D/2D van der waals heterojunction based on covalent organic frameworks for highly efficient solar energy catalysis. *Nano-Micro Lett.* **15**(1), 132 (2023). <https://doi.org/10.1007/s40820-023-01100-x>
  52. T. Zhang, C. Gao, W. Huang, Y. Chen, Y. Wang et al., Covalent organic framework as a novel electrochemical platform for highly sensitive and stable detection of lead. *Talanta* **188**, 578–583 (2018). <https://doi.org/10.1016/j.talanta.2018.06.032>
  53. F. Pan, C. Tong, Z. Wang, H. Han, P. Liu et al., Nanocomposite based on graphene and intercalated covalent organic frameworks with hydrosulphonyl groups for electrochemical determination of heavy metal ions. *Microchim. Acta* **188**(9), 295 (2021). <https://doi.org/10.1007/s00604-021-04956-1>
  54. H. Wang, J. Zhao, Y. Li, Y. Cao, Z. Zhu et al., Aqueous two-phase interfacial assembly of COF membranes for water desalination. *Nano-Micro Lett.* **14**(1), 216 (2022). <https://doi.org/10.1007/s40820-022-00968-5>
  55. O. Yildirim, B. Derkus, Triazine-based 2D covalent organic frameworks improve the electrochemical performance of enzymatic biosensors. *J. Mater. Sci.* **55**(7), 3034–3044 (2019). <https://doi.org/10.1007/s10853-019-04254-5>
  56. X. Liu, M. Hu, M. Wang, Y. Song, N. Zhou et al., Novel nano-architecture of Co-MOF-on-TPN-COF hybrid: ultralowly sensitive bioplatfrom of electrochemical aptasensor toward ampicillin. *Biosens. Bioelectron.* **123**, 59–68 (2019). <https://doi.org/10.1016/j.bios.2018.09.089>





57. Y. Cao, R. Wu, Y. Zhou, D. Jiang, W. Zhu, A bioinspired photocatalysis and electrochemiluminescence scaffold for simultaneous degradation and in situ evaluation. *Adv. Funct. Mater.* **32**(31), 2203005 (2022). <https://doi.org/10.1002/adfm.202203005>
58. J.L. Zhang, L.Y. Yao, Y. Yang, W.B. Liang, R. Yuan et al., Conductive covalent organic frameworks with conductivity- and pre-reduction-enhanced electrochemiluminescence for ultrasensitive biosensor construction. *Anal. Chem.* **94**(8), 3685–3692 (2022). <https://doi.org/10.1021/acs.analchem.1c05436>
59. Y.J. Li, W.R. Cui, Q.Q. Jiang, Q. Wu, R.P. Liang et al., A general design approach toward covalent organic frameworks for highly efficient electrochemiluminescence. *Nat. Commun.* **12**(1), 4735 (2021). <https://doi.org/10.1038/s41467-021-25013-8>
60. Y. Sun, G.I.N. Waterhouse, L. Xu, X. Qiao, Z. Xu, Three-dimensional electrochemical sensor with covalent organic framework decorated carbon nanotubes signal amplification for the detection of furazolidone. *Sens. Actuators B Chem.* **321**, 128501 (2020). <https://doi.org/10.1016/j.snb.2020.128501>
61. L. Wang, Y. Song, Y. Luo, L. Wang, A novel covalent organic framework with multiple adsorption sites for removal of Hg<sup>2+</sup> and sensitive detection of nitrofur. *J. Ind. Eng. Chem.* **106**, 374–381 (2022). <https://doi.org/10.1016/j.jiec.2021.11.014>
62. D. Li, H. Zhao, G. Wang, R. Liu, L. Bai, Room-temperature ultrasonic-assisted self-assembled synthesis of silkworm cocoon-like COFs@GCNTs composite for sensitive detection of diuron in food samples. *Food Chem.* **418**, 135999 (2023). <https://doi.org/10.1016/j.foodchem.2023.135999>
63. B. Liu, H. Guo, L. Sun, Z. Pan, L. Peng et al., Electrochemical sensor based on covalent organic frameworks/MWCNT for simultaneous detection of catechol and hydroquinone. *Colloids Surf. A* **639**, 128335 (2022). <https://doi.org/10.1016/j.colsurfa.2022.128335>
64. H. Guo, B. Liu, Z. Pan, L. Sun, L. Peng et al., Electrochemical determination of dopamine and uric acid with covalent organic frameworks and Ox-MWCNT co-modified glassy carbon electrode. *Colloids Surf. A* **648**, 129316 (2022). <https://doi.org/10.1016/j.colsurfa.2022.129316>
65. Z. Pan, Y. Wei, H. Guo, B. Liu, L. Sun et al., Sensitive detection of sulfamethoxazole by an electrochemical sensing platform with a covalent organic framework in situ grown on polyaniline. *Microporous Mesoporous Mater.* **348**, 112409 (2023). <https://doi.org/10.1016/j.micromeso.2022.112409>
66. S. Lu, S. Wang, P. Wu, D. Wang, J. Yi et al., A composite prepared from covalent organic framework and gold nanoparticles for the electrochemical determination of enrofloxacin. *Adv. Powder Technol.* **32**(6), 2106–2115 (2021). <https://doi.org/10.1016/j.appt.2021.04.025>
67. T. Zhang, Y. Chen, W. Huang, Y. Wang, X. Hu, A novel AuNPs-doped COFs composite as electrochemical probe for chlorogenic acid detection with enhanced sensitivity and stability. *Sens. Actuators B Chem.* **276**, 362–369 (2018). <https://doi.org/10.1016/j.snb.2018.08.132>
68. Q. Guan, H. Guo, R. Xue, M. Wang, N. Wu et al., Electrochemical sensing platform based on covalent organic framework materials and gold nanoparticles for high sensitivity determination of theophylline and caffeine. *Microchim. Acta* **188**(3), 85 (2021). <https://doi.org/10.1007/s00604-021-04744-x>
69. X. Zhang, J. Zhu, Z. Wu, W. Wen, X. Zhang et al., Electrochemical sensor based on confined synthesis of gold nanoparticles@covalent organic frameworks for the detection of bisphenol A. *Anal. Chim. Acta* **1239**, 340743 (2023). <https://doi.org/10.1016/j.aca.2022.340743>
70. H. Zhao, K. Shi, C. Zhang, J. Ren, M. Cui et al., Spherical COFs decorated with gold nanoparticles and multiwalled carbon nanotubes as signal amplifier for sensitive electrochemical detection of doxorubicin. *Microchem. J.* **182**, 107865 (2022). <https://doi.org/10.1016/j.microc.2022.107865>
71. R. Chen, X. Peng, Y. Song, Y. Du, A paper-based electrochemical sensor based on PtNP/COFTFPB-DH<sub>2</sub>DS@rGO for sensitive detection of furazolidone. *Biosensors* **12**(10), 904 (2022). <https://doi.org/10.3390/bios12100904>
72. Q. Guan, H. Guo, R. Xue, M. Wang, X. Zhao et al., Electrochemical sensor based on covalent organic frameworks-MWCNT-NH<sub>2</sub>/AuNPs for simultaneous detection of dopamine and uric acid. *J. Electroanal. Chem.* **880**, 114932 (2021). <https://doi.org/10.1016/j.jelechem.2020.114932>
73. Z. Pan, H. Guo, B. Liu, L. Sun, Y. Chen et al., A sensitive electrochemical sensing platform based on nitrogen-rich covalent organic framework for simultaneous detection of guanine and adenine. *Microporous Mesoporous Mater.* **340**, 112030 (2022). <https://doi.org/10.1016/j.micromeso.2022.112030>
74. W. Wei, S. Zhou, D.D. Ma, Q. Li, M. Ran et al., Ultrathin conductive bithiazole-based covalent organic framework nanosheets for highly efficient electrochemical biosensing. *Adv. Funct. Mater.* **33**(36), 2302917 (2023). <https://doi.org/10.1002/adfm.202302917>
75. X. Lin, Y. Deng, Y. He, J. Chen, S. Hu, Construction of hydrophilic N, O-rich carboxylated triazine-covalent organic frameworks for the application in selective simultaneous electrochemical detection. *Appl. Surf. Sci.* **545**, 149047 (2021). <https://doi.org/10.1016/j.apsusc.2021.149047>
76. X. Tan, Y. Fan, S. Wang, Y. Wu, W. Shi, Ultrasensitive and highly selective electrochemical sensing of sodium picrate by dihydroxylatopillar[6]arene-modified gold nanoparticles and cationic pillar[6]arene functionalized covalent organic framework. *Electrochim. Acta* **335**, 135706 (2020). <https://doi.org/10.1016/j.electacta.2020.135706>
77. Y. Xiao, N. Wu, L. Wang, L. Chen, A novel paper-based electrochemical biosensor based on N, O-rich covalent organic frameworks for carbaryl detection. *Biosensors* **12**(10), 899 (2022). <https://doi.org/10.3390/bios12100899>
78. L. Wang, H. Liang, M. Xu, L. Wang, Y. Xie et al., Ratiometric electrochemical biosensing based on double-enzymes loaded on two-dimensional dual-pore COFETTA-TPAL.

- Sens. Actuators B Chem. **298**, 126859 (2019). <https://doi.org/10.1016/j.snb.2019.126859>
79. X. Zha, X. Sun, H. Chu, Y. Wang, Synthesis of bimetallic covalent organic framework nanocomposite for enhanced electrochemical detection of gallic acid. *Colloids Surf. A* **651**, 129748 (2022). <https://doi.org/10.1016/j.colsurfa.2022.129748>
  80. H. Chu, X. Sun, X. Zha, Y. Zhang, Y. Wang, Synthesis of core-shell structured metal oxide@covalent organic framework composites as a novel electrochemical platform for dopamine sensing. *Colloids Surf. A* **648**, 129238 (2022). <https://doi.org/10.1016/j.colsurfa.2022.129238>
  81. Y. Xie, M. Xu, L. Wang, H. Liang, L. Wang et al., Iron-porphyrin-based covalent-organic frameworks for electrochemical sensing  $\text{H}_2\text{O}_2$  and pH. *Mater. Sci. Eng. C* **112**, 110864 (2020). <https://doi.org/10.1016/j.msec.2020.110864>
  82. C. Zhang, L. Fan, J. Ren, M. Cui, N. Li et al., Facile synthesis of surface functionalized  $\text{Pd}^{2+}$ @P-CDP/COFs for highly sensitive detection of norfloxacin drug based on the host-guest interaction. *J. Pharm. Biomed. Anal.* **219**, 114956 (2022). <https://doi.org/10.1016/j.jpba.2022.114956>
  83. L. Wang, Y. Xie, Y. Yang, H. Liang, L. Wang et al., Electroactive covalent organic frameworks/carbon nanotubes composites for electrochemical sensing. *ACS Appl. Nano Mater.* **3**(2), 1412–1419 (2020). <https://doi.org/10.1021/acsanm.9b02257>
  84. N. Wu, L. Wang, Y. Xie, Y. Du, Y. Song et al., Double signal ratiometric electrochemical riboflavin sensor based on macroporous carbon/electroactive thionine-contained covalent organic framework. *J. Colloids Interface Sci.* **608**(1), 219–226 (2022). <https://doi.org/10.1016/j.jcis.2021.09.162>
  85. M. Xu, L. Wang, Y. Xie, Y. Song, L. Wang, Ratiometric electrochemical sensing and biosensing based on multiple redox-active state COFDHTA-TTA. *Sens. Actuators B Chem.* **281**, 1009–1015 (2019). <https://doi.org/10.1016/j.snb.2018.11.032>
  86. Y.H. Pang, Y.Y. Wang, X.F. Shen, J.Y. Qiao, Covalent organic framework modified carbon cloth for ratiometric electrochemical sensing of bisphenol A and S. *Microchim. Acta* **189**(5), 189 (2022). <https://doi.org/10.1007/s00604-022-05297-3>
  87. M.R. Jalali Sarvestani, T. Madrakian, A. Afkhami, Ultra-trace levels voltammetric determination of  $\text{Pb}^{2+}$  in the presence of  $\text{Bi}^{3+}$  at food samples by a  $\text{Fe}_3\text{O}_4$ @schiff base network1 modified glassy carbon electrode. *Talanta* **250**, 123716 (2022). <https://doi.org/10.1016/j.talanta.2022.123716>
  88. L. Wang, Y. Yang, H. Liang, N. Wu, X. Peng et al., A novel N, S-rich COF and its derived hollow N, S-doped carbon@Pd nanorods for electrochemical detection of  $\text{Hg}^{2+}$  and paracetamol. *J. Hazard. Mater.* **409**, 124528 (2021). <https://doi.org/10.1016/j.jhazmat.2020.124528>
  89. L. Pei, J. Su, H. Yang, Y. Wu, Y. Du et al., A novel covalent-organic framework for highly sensitive detection of  $\text{Cd}^{2+}$ ,  $\text{Pb}^{2+}$ ,  $\text{Cu}^{2+}$  and  $\text{Hg}^{2+}$ . *Microporous Mesoporous Mater.* **333**, 111742 (2022). <https://doi.org/10.1016/j.micromeso.2022.111742>
  90. J. Han, L. Pei, Y. Du, Y. Zhu, Tripolycyanamide-2,4,6-triformyl pyrogallol covalent organic frameworks with many coordination sites for detection and removal of heavy metal ions. *J. Ind. Eng. Chem.* **107**, 53–60 (2022). <https://doi.org/10.1016/j.jiec.2021.11.027>
  91. L. Yu, L. Sun, Q. Zhang, J. Zhang, B. Yang et al., Highly efficient determination of  $\text{Mn}^{2+}$  in chinese liquor by using a novel electrochemical sensor based on  $\text{TiO}_2\text{-NH}_2$ @covalent organic framework nanocomposites. *Anal. Methods* **15**(21), 2622–2630 (2023). <https://doi.org/10.1039/d3ay00222e>
  92. S. Feng, M. Yan, Y. Xue, J. Huang, X. Yang, Electrochemical immunosensor for cardiac troponin I detection based on covalent organic framework and enzyme-catalyzed signal amplification. *Anal. Chem.* **93**(40), 13572–13579 (2021). <https://doi.org/10.1021/acs.analchem.1c02636>
  93. T. Zhang, N. Ma, A. Ali, Q. Wei, D. Wu et al., Electrochemical ultrasensitive detection of cardiac troponin I using covalent organic frameworks for signal amplification. *Biosens. Bioelectron.* **119**, 176–181 (2018). <https://doi.org/10.1016/j.bios.2018.08.020>
  94. H. Liang, H. Xu, Y. Zhao, J. Zheng, H. Zhao et al., Ultrasensitive electrochemical sensor for prostate specific antigen detection with a phosphorene platform and magnetic covalent organic framework signal amplifier. *Biosens. Bioelectron.* **144**, 111691 (2019). <https://doi.org/10.1016/j.bios.2019.111691>
  95. T.Z. Liu, R. Hu, X. Zhang, K.L. Zhang, Y. Liu et al., Metal-organic framework nanomaterials as novel signal probes for electron transfer mediated ultrasensitive electrochemical immunoassay. *Anal. Chem.* **88**(24), 12516–12523 (2016). <https://doi.org/10.1021/acs.analchem.6b04191>
  96. H. Boyacıoğlu, B.B. Yola, C. Karaman, O. Karaman, N. Atar et al., A novel electrochemical kidney injury molecule-1 (KIM-1) immunosensor based covalent organic frameworks-gold nanoparticles composite and porous  $\text{NiCo}_2\text{S}_4$ @ $\text{CeO}_2$  microspheres: the monitoring of acute kidney injury. *Appl. Surf. Sci.* **578**, 152093 (2022). <https://doi.org/10.1016/j.apsusc.2021.152093>
  97. Y. Chen, S. Wang, J. Ren, H. Zhao, M. Cui et al., Electrocatalysis of copper sulfide nanoparticle-engineered covalent organic frameworks for ratiometric electrochemical detection of amyloid-beta oligomer. *Anal. Chem.* **94**(32), 11201–11208 (2022). <https://doi.org/10.1021/acs.analchem.2c01602>
  98. H. Liu, S. Ma, G. Ning, R. Zhang, H. Liang et al., A “peptide-target-aptamer” electrochemical biosensor for norovirus detection using a black phosphorous nanosheet@ $\text{Ti}_3\text{C}_2\text{-Mxene}$  nanohybrid and magnetic covalent organic framework. *Talanta* **258**, 124433 (2023). <https://doi.org/10.1016/j.talanta.2023.124433>
  99. Z. Chen, M. Yang, Z. Li, W. Liao, B. Chen et al., Highly sensitive and convenient aptasensor based on Au NPs@Ce-TpBpy COF for quantitative determination of zearalenone. *RSC Adv.* **12**(27), 17312–17320 (2022). <https://doi.org/10.1039/d2ra02093a>
  100. Z. Song, J. Song, F. Gao, X. Chen, Q. Wang et al., Novel electroactive ferrocene-based covalent organic frameworks towards electrochemical label-free aptasensors for the



- detection of cardiac troponin i. *Sens. Actuators B Chem.* **368**, 132205 (2022). <https://doi.org/10.1016/j.snb.2022.132205>
101. Q.Q. Zhu, W.W. Zhang, H.W. Zhang, R. Yuan, H. He, Elaborately manufacturing an electrochemical aptasensor based on gold nanoparticle/COF composites for amplified detection performance. *J. Mater. Chem. C* **8**(47), 16984–16991 (2020). <https://doi.org/10.1039/d0tc04202a>
  102. Q.Q. Zhu, H.K. Li, X.L. Sun, Z.Y. Han, J. Sun et al., Rational incorporation of covalent organic framework/carbon nanotube (COF/CNT) composites for electrochemical aptasensing of ultra-trace atrazine. *J. Mater. Chem. C* **9**(25), 8043–8050 (2021). <https://doi.org/10.1039/d1tc01506k>
  103. M. Wang, M. Hu, J. Liu, C. Guo, D. Peng et al., Covalent organic framework-based electrochemical aptasensors for the ultrasensitive detection of antibiotics. *Biosens. Bioelectron.* **132**, 8–16 (2019). <https://doi.org/10.1016/j.bios.2019.02.040>
  104. X. Yan, Y. Song, J. Liu, N. Zhou, C. Zhang et al., Two-dimensional porphyrin-based covalent organic framework: a novel platform for sensitive epidermal growth factor receptor and living cancer cell detection. *Biosens. Bioelectron.* **126**, 734–742 (2019). <https://doi.org/10.1016/j.bios.2018.11.047>
  105. Z. He, J. Goulas, E. Parker, Y. Sun, X.D. Zhou et al., Review on covalent organic frameworks and derivatives for electrochemical and photocatalytic CO<sub>2</sub> reduction. *Catal. Today* **409**, 103–118 (2023). <https://doi.org/10.1016/j.cattod.2022.04.021>
  106. T. Zhang, Y. Song, Y. Xing, Y. Gu, X. Yan et al., The synergistic effect of Au-COF nanosheets and artificial peroxidase Au@ZIF-8(NiPd) rhombic dodecahedra for signal amplification for biomarker detection. *Nanoscale* **11**(42), 20221–20227 (2019). <https://doi.org/10.1039/c9nr07190c>
  107. Y. Chen, W. Li, X.H. Wang, R.Z. Gao, A.N. Tang et al., Green synthesis of covalent organic frameworks based on reaction media. *Mater. Chem. Front.* **5**(3), 1253–1267 (2021). <https://doi.org/10.1039/d0qm00801j>
  108. H. Wang, Z. Zeng, P. Xu, L. Li, G. Zeng et al., Recent progress in covalent organic framework thin films: fabrications, applications and perspectives. *Chem. Soc. Rev.* **48**(2), 488–516 (2019). <https://doi.org/10.1039/c8cs00376a>
  109. X. Huang, L. Li, S. Zhao, L. Tong, Z. Li et al., MOF-like 3D graphene-based catalytic membrane fabricated by one-step laser scribing for robust water purification and green energy production. *Nano-Micro Lett.* **14**(1), 174 (2022). <https://doi.org/10.1007/s40820-022-00923-4>
  110. J. Qiao, X. Zhang, C. Liu, L. Lyu, Y. Yang et al., Non-magnetic bimetallic MOF-derived porous carbon-wrapped TiO<sub>2</sub>/ZrTiO<sub>4</sub> composites for efficient electromagnetic wave absorption. *Nano-Micro Lett.* **13**(1), 75 (2021). <https://doi.org/10.1007/s40820-021-00606-6>
  111. C. Qiu, K. Qian, J. Yu, M. Sun, S. Cao et al., MOF-transformed In<sub>2</sub>O<sub>3-x</sub>@C nanocorn electrocatalyst for efficient CO<sub>2</sub> reduction to HCOOH. *Nano-Micro Lett.* **14**(1), 167 (2022). <https://doi.org/10.1007/s40820-022-00913-6>
  112. V. Schroeder, S. Savagatrup, M. He, S. Lin, T.M. Swager, Carbon nanotube chemical sensors. *Chem. Rev.* **119**(1), 599–663 (2019). <https://doi.org/10.1021/acs.chemrev.8b00340>
  113. Z. Wang, L. Dong, W. Huang, H. Jia, Q. Zhao et al., Simultaneously regulating uniform Zn<sup>2+</sup> flux and electron conduction by mof/rgo interlayers for high-performance Zn anodes. *Nano-Micro Lett.* **13**(1), 73 (2021). <https://doi.org/10.1007/s40820-021-00594-7>
  114. H. Chu, X. Sun, X. Zha, S.U. Khan, Y. Wang, Ultrasensitive electrochemical detection of butylated hydroxy anisole via metalloporphyrin covalent organic frameworks possessing variable catalytic active sites. *Biosensors* **12**(11), 975 (2022). <https://doi.org/10.3390/bios12110975>
  115. T. Yang, R. Yu, Y. Yan, H. Zeng, S. Luo et al., A review of ratiometric electrochemical sensors: from design schemes to future prospects. *Sens. Actuators B Chem.* **274**, 501–516 (2018). <https://doi.org/10.1016/j.snb.2018.07.138>
  116. Y. Cao, C. Ma, J.J. Zhu, DNA technology-assisted signal amplification strategies in electrochemiluminescence bioanalysis. *J. Anal. Test.* **5**(2), 95–111 (2021). <https://doi.org/10.1007/s41664-021-00175-y>
  117. J. Cao, P. Ouyang, S. Yu, F. Shi, C. Ren et al., Hedgehog-like Bi<sub>2</sub>S<sub>3</sub> nanostructures: a novel composite soft template route to the synthesis and sensitive electrochemical immunoassay of the liver cancer biomarker. *Chem. Commun.* **57**(14), 1766–1769 (2021). <https://doi.org/10.1039/d0cc07572h>
  118. T. Han, Y. Cao, H.Y. Chen, J.J. Zhu, Versatile porous nanomaterials for electrochemiluminescence biosensing: recent advances and future perspective. *J. Electroanal. Chem.* **902**, 115821 (2021). <https://doi.org/10.1016/j.jelechem.2021.115821>
  119. Y. Zhang, B.S. Lai, M. Juhas, Recent advances in aptamer discovery and applications. *Molecules* **24**(5), 941 (2019). <https://doi.org/10.3390/molecules24050941>
  120. Y.W. Zhang, Y. Cao, C.J. Mao, D. Jiang, W. Zhu, An iron(III)-based metal-organic gel-catalyzed dual electrochemiluminescence system for cytosensing and in situ evaluation of the VEGF165 subtype. *Anal. Chem.* **94**(9), 4095–4102 (2022). <https://doi.org/10.1021/acs.analchem.2c00032>
  121. S.M. Khoshfetrat, K. Fasihi, F. Moradnia, H. Kamil Zaidan, E. Sanchooli, A label-free multicolor colorimetric and fluorescence dual mode biosensing of HIV-1 DNA based on the bifunctional NiFe<sub>2</sub>O<sub>4</sub>@UiO-66 nanozyme. *Anal. Chim. Acta* **1252**, 341073 (2023). <https://doi.org/10.1016/j.aca.2023.341073>
  122. S.M. Khoshfetrat, P.S. Dorraji, L. Fotouhi, M. Hosseini, F. Khatami et al., Enhanced electrochemiluminescence biosensing of gene-specific methylation in thyroid cancer patients' plasma based integrated graphitic carbon nitride-encapsulated metal-organic framework nanozyme optimized by central composite design. *Sens. Actuators B Chem.* **364**, 131895 (2022). <https://doi.org/10.1016/j.snb.2022.131895>
  123. S.M. Khoshfetrat, P. Seyed Dorraji, M. Shayan, F. Khatami, K. Omidfar, Smartphone-based electrochemiluminescence for visual simultaneous detection of RASSF1A and SLC5A8 tumor suppressor gene methylation in thyroid

- cancer patient plasma. *Anal. Chem.* **94**(22), 8005–8013 (2022). <https://doi.org/10.1021/acs.analchem.2c01132>
124. A. Ahmadi, S.M. Khoshfetrat, Z. Mirzaeizadeh, S. Kabiri, J. Rezaie et al., Electrochemical immunosensor for determination of cardiac troponin i using two-dimensional metal-organic framework/Fe<sub>3</sub>O<sub>4</sub>-COOH nanosheet composites loaded with thionine and pCTAB/DES modified electrode. *Talanta* **237**, 122911 (2022). <https://doi.org/10.1016/j.talanta.2021.122911>
  125. S.M. Khoshfetrat, P. Hashemi, A. Afkhami, A. Hajian, H. Bagheri, Cascade electrochemiluminescence-based integrated graphitic carbon nitride-encapsulated metal-organic framework nanozyme for prostate-specific antigen biosensing. *Sens. Actuators B Chem.* **348**, 130658 (2021). <https://doi.org/10.1016/j.snb.2021.130658>
  126. H. Zhao, F. Wang, L. Cui, X. Xu, X. Han et al., Composition optimization and microstructure design in mofs-derived magnetic carbon-based microwave absorbers: a review. *Nano-Micro Lett.* **13**(1), 208 (2021). <https://doi.org/10.1007/s40820-021-00734-z>
  127. Z. Zhang, Z. Cai, Z. Wang, Y. Peng, L. Xia et al., A review on metal-organic framework-derived porous carbon-based novel microwave absorption materials. *Nano-Micro Lett.* **13**(1), 56 (2021). <https://doi.org/10.1007/s40820-020-00582-3>
  128. X. Zhang, J. Qiao, Y. Jiang, F. Wang, X. Tian et al., Carbon-based MOF derivatives: emerging efficient electromagnetic wave absorption agents. *Nano-Micro Lett.* **13**(1), 135 (2021). <https://doi.org/10.1007/s40820-021-00658-8>
  129. R. Luo, H. Lv, Q. Liao, N. Wang, J. Yang et al., Intrarecticular charge transfer regulated electrochemiluminescence of donor-acceptor covalent organic frameworks. *Nat. Commun.* **12**(1), 6808 (2021). <https://doi.org/10.1038/s41467-021-27127-5>
  130. W.R. Cui, Y.J. Li, Q.Q. Jiang, Q. Wu, R.P. Liang et al., Tunable covalent organic framework electrochemiluminescence from non-electroluminescent monomers. *Cell Rep. Phys. Sci.* **3**(2), 100630 (2022). <https://doi.org/10.1016/j.xcrp.2021.100630>
  131. W.J. Zeng, K. Wang, W.B. Liang, Y.Q. Chai, R. Yuan et al., Covalent organic frameworks as micro-reactors: confinement-enhanced electrochemiluminescence. *Chem. Sci.* **11**(21), 5410–5414 (2020). <https://doi.org/10.1039/d0sc01817a>
  132. Y. Cao, W. Zhu, H. Wei, C. Ma, Y. Lin et al., Stable and monochromatic all-inorganic halide perovskite assisted by hollow carbon nitride nanosphere for ratiometric electrochemiluminescence bioanalysis. *Anal. Chem.* **92**(5), 4123–4130 (2020). <https://doi.org/10.1021/acs.analchem.0c00070>
  133. Y.J. Li, W.R. Cui, Q.Q. Jiang, R.P. Liang, X.J. Li et al., Arousing electrochemiluminescence out of non-electroluminescent monomers within covalent organic frameworks. *ACS Appl. Mater. Interfaces* **13**(40), 47921–47931 (2021). <https://doi.org/10.1021/acsami.1c12958>
  134. W.R. Cui, Y.J. Li, Q.Q. Jiang, Q. Wu, Q.X. Luo et al., Covalent organic frameworks as advanced uranyl electrochemiluminescence monitoring platforms. *Anal. Chem.* **93**(48), 16149–16157 (2021). <https://doi.org/10.1021/acs.analchem.1c03907>
  135. S. Carrara, A. Aliprandi, C.F. Hogan, L. De Cola, Aggregation-induced electrochemiluminescence of platinum(II) complexes. *J. Am. Chem. Soc.* **139**(41), 14605–14610 (2017). <https://doi.org/10.1021/jacs.7b07710>
  136. X. Wei, M.J. Zhu, Z. Cheng, M. Lee, H. Yan et al., Aggregation-induced electrochemiluminescence of carboranyl carbazoles in aqueous media. *Angew. Chem. Int. Ed.* **58**(10), 3162–3166 (2019). <https://doi.org/10.1002/anie.201900283>
  137. T. Han, Y. Cao, J. Wang, J. Jiao, Y. Song et al., Crystallization-induced enhanced electrochemiluminescence from a new tris(bipyridine)ruthenium(II) derivative. *Adv. Funct. Mater.* **33**(12), 2212394 (2023). <https://doi.org/10.1002/adfm.202212394>
  138. Q.X. Luo, W.R. Cui, Y.J. Li, Y.J. Cai, X.L. Mao et al., Construction of sp<sup>2</sup> carbon-conjugated covalent organic frameworks for framework-induced electrochemiluminescence. *ACS Appl. Electron. Mater.* **3**(10), 4490–4497 (2021). <https://doi.org/10.1021/acsaem.1c00636>
  139. S. Li, X. Ma, C. Pang, M. Wang, G. Yin et al., Novel chloramphenicol sensor based on aggregation-induced electrochemiluminescence and nanozyme amplification. *Biosens. Bioelectron.* **176**, 112944 (2021). <https://doi.org/10.1016/j.bios.2020.112944>
  140. S. Li, C. Pang, X. Ma, Y. Wu, M. Wang et al., Aggregation-induced electrochemiluminescence and molecularly imprinted polymer based sensor with Fe<sub>3</sub>O<sub>4</sub>@Pt nanoparticle amplification for ultrasensitive ciprofloxacin detection. *Microchem. J.* **178**, 107345 (2022). <https://doi.org/10.1016/j.microc.2022.107345>
  141. J.L. Zhang, Y. Yang, W.B. Liang, L.Y. Yao, R. Yuan et al., Highly stable covalent organic framework nanosheets as a new generation of electrochemiluminescence emitters for ultrasensitive microRNA detection. *Anal. Chem.* **93**(6), 3258–3265 (2021). <https://doi.org/10.1021/acs.analchem.0c04931>
  142. L. Cui, C.Y. Zhu, J. Hu, X.M. Meng, M. Jiang et al., Construction of a dual-mode biosensor for electrochemiluminescent and electrochemical sensing of alkaline phosphatase. *Sens. Actuators B Chem.* **374**, 132779 (2023). <https://doi.org/10.1016/j.snb.2022.132779>
  143. Y. Yang, H. Jiang, J. Li, J. Zhang, S.Z. Gao et al., Highly stable Ru-complex-based metal-covalent organic frameworks as novel type of electrochemiluminescence emitters for ultrasensitive biosensing. *Mater. Horiz.* **10**, 3005–3013 (2023). <https://doi.org/10.1039/d3mh00260h>
  144. L. Song, W. Gao, S. Wang, H. Bi, S. Deng et al., Construction of an aminated-linked covalent organic framework-based electrochemiluminescent sensor for enantioselective sensing of phenylalanine. *Sens. Actuators B Chem.* **373**, 132751 (2022). <https://doi.org/10.1016/j.snb.2022.132751>
  145. L. Song, W. Gao, Q. Han, Y. Huang, L. Cui et al., Construction of an aggregation-induced electrochemiluminescent sensor based on an aminated-linked covalent organic framework for sensitive detection of glutathione in human serum. *Chem.*





- Commun. **58**(75), 10524–10527 (2022). <https://doi.org/10.1039/d2cc03753j>
146. X.L. Mao, Q.X. Luo, Y.J. Cai, X. Liu, Q.Q. Jiang et al., Structural isomerism of covalent organic frameworks causing different electrochemiluminescence effects and its application for the detection of arsenic. *Anal. Chem.* **95**(28), 10803–10811 (2023). <https://doi.org/10.1021/acs.analchem.3c02082>
147. Q.Q. Jiang, Y.J. Li, Q. Wu, X. Wang, Q.X. Luo et al., Guest molecular assembly strategy in covalent organic frameworks for electrochemiluminescence sensing of uranyl. *Anal. Chem.* **95**(22), 8696–8705 (2023). <https://doi.org/10.1021/acs.analchem.3c01299>
148. Q.X. Luo, Y.J. Cai, X.L. Mao, Y.J. Li, C.R. Zhang et al., Tuned-potential covalent organic framework electrochemiluminescence platform for lutetium analysis. *J. Electroanal. Chem.* **923**, 116831 (2022). <https://doi.org/10.1016/j.jelechem.2022.116831>
149. X. Ma, C. Pang, S. Li, Y. Xiong, J. Li et al., Synthesis of Zr-coordinated amide porphyrin-based two-dimensional covalent organic framework at liquid–liquid interface for electrochemical sensing of tetracycline. *Biosens. Bioelectron.* **146**, 111734 (2019). <https://doi.org/10.1016/j.bios.2019.111734>
150. L. Li, W. Zhao, Y. Wang, X. Liu, P. Jiang et al., Gold nano-cluster-confined covalent organic frameworks as bifunctional probes for electrochemiluminescence and colorimetric dual-response sensing of  $\text{Pb}^{2+}$ . *J. Hazard. Mater.* **457**, 131558 (2023). <https://doi.org/10.1016/j.jhazmat.2023.131558>
151. R. Ma, J. Jiang, Y. Ya, Y. Lin, Y. Zhou et al., A carbon dot-based nanoscale covalent organic framework as a new emitter combined with a CRISPR/Cas12a-mediated electrochemiluminescence biosensor for ultrasensitive detection of bisphenol a. *Analyst* **148**(6), 1362–1370 (2023). <https://doi.org/10.1039/d3an00024a>
152. L. Shen, Y.W. Wang, H.Y. Shan, J. Chen, A.J. Wang et al., Covalent organic framework linked with amination luminol derivative as enhanced ECL luminophore for ultrasensitive analysis of cytochrome C. *Anal. Methods* **14**(46), 4767–4774 (2022). <https://doi.org/10.1039/d2ay01208a>